Cell Reports

Article

Induction of OCT2 contributes to regulate the gene expression program in human neutrophils activated via TLR8

Graphical abstract

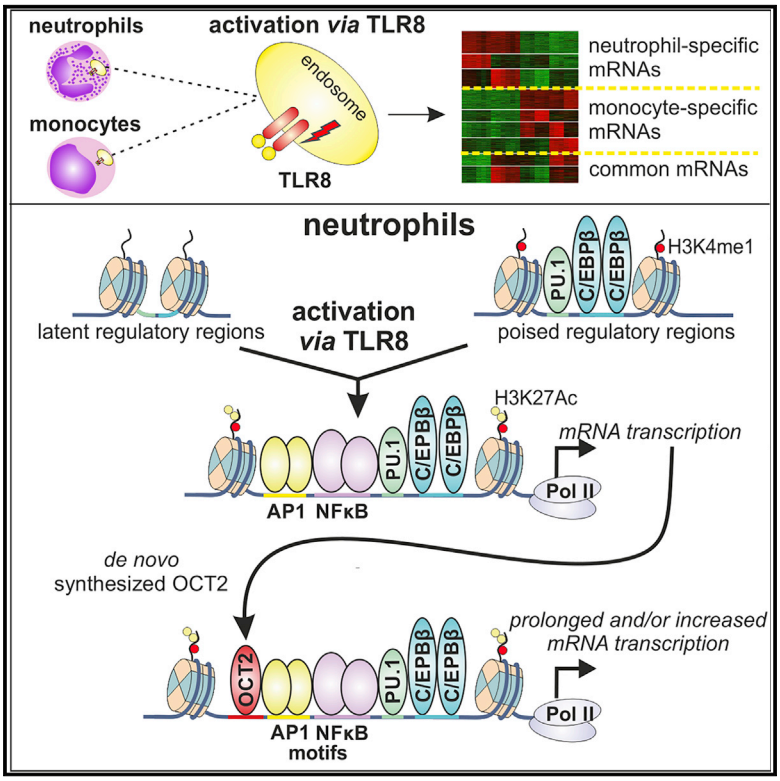

Highlights

- Activation of neutrophils via TLR8 promotes a cell-specific transcriptional program
- OCT motifs emerge from H3K27Ac, PU.1, and C/EBPβ ChIP-seq in R848-treated neutrophils
- OCT motifs bind *de novo* synthesized OCT2 in TLR8-activated human neutrophils
- OCT2 acts as a transcriptional amplifier in TLR8-activated human neutrophils

Authors

Nicola Tamassia, Francisco Bianchetto-Aguilera, Sara Gasperini, ..., Renato Ostuni, Gioacchino Natoli, Marco A. Cassatella

Correspondence

nicola.tamassia@univr.it (N.T.), marco.cassatella@univr.it (M.A.C.)

In brief

Tamassia et al. report that activation of neutrophils via TLR8 promotes a cell-specific transcriptional program, as well as increased H3K27Ac levels and PU.1 and C/EBPβ DNA binding. By ChIP-seq, the authors also reveal a concomitant enrichment of OCT motifs to which *de novo* synthesized OCT2 binds and functions as a transcriptional amplifier.

Tamassia et al., 2021, Cell Reports *35*, 109143
May 18, 2021
https://doi.org/10.1016/j.celrep.2021.109143

CellPress

Cell Reports

CellPress
OPEN ACCESS

Article

Induction of OCT2 contributes to regulate the gene expression program in human neutrophils activated via TLR8

Nicola Tamassia,[1,6,*] Francisco Bianchetto-Aguilera,[1,6] Sara Gasperini,[1] Sara Polletti,[2] Elisa Gardiman,[1] Renato Ostuni,[3,4] Gioacchino Natoli,[2,5] and Marco A. Cassatella[1,7,*]

[1]Department of Medicine, Section of General Pathology, University of Verona, Verona 37134, Italy
[2]Department of Experimental Oncology, European Institute of Oncology IRCCS (IEO), Milan 20139, Italy
[3]San Raffaele Telethon Institute for Gene Therapy (SR-TIGET), IRCCS San Raffaele Scientific Institute, Milan 20132, Italy
[4]Vita-Salute San Raffaele University, Milan 20132, Italy
[5]Department of Biomedical Sciences, Humanitas University, Milan 20090, Italy
[6]These authors contributed equally
[7]Lead contact
*Correspondence: nicola.tamassia@univr.it (N.T.), marco.cassatella@univr.it (M.A.C.)
https://doi.org/10.1016/j.celrep.2021.109143

SUMMARY

The transcription factors (TFs) that regulate inducible genes in activated neutrophils are not yet completely characterized. Herein, we show that the genomic distribution of the histone modification H3K27Ac, as well as PU.1 and C/EBPβ, two myeloid-lineage-determining TFs (LDTFs), significantly changes in human neutrophils treated with R848, a ligand of Toll-like receptor 8 (TLR8). Interestingly, differentially acetylated and LDTF-marked regions reveal an over-representation of OCT-binding motifs that are selectively bound by OCT2/POU2F2. Analysis of OCT2 genomic distribution in primary neutrophils and of OCT2-depletion in HL-60-differentiated neutrophils proves the requirement for OCT2 in contributing to promote, along with nuclear factor κB (NF-κB) and activator protein 1 (AP-1), the TLR8-induced gene expression program in neutrophils. Altogether, our data demonstrate that neutrophils, upon activation via TLR8, profoundly reprogram their chromatin status, ultimately displaying cell-specific, prolonged transcriptome changes. Data also show an unexpected role for OCT2 in amplifying the transcriptional response to TLR8-mediated activation.

INTRODUCTION

Neutrophils are key cellular players of the innate immune system because they perform frontline defense against pathogens (Ley et al., 2018). In addition, accumulating evidence that has emerged in the past years indicates that neutrophils are able to exert an array of complex functions involved in the modulation of both innate and adaptive immune responses (Ley et al., 2018; Scapini and Cassatella, 2014). These novel functions not only include migration into lymph nodes, the capacity to present antigens, the release of neutrophil extracellular traps (NETs) and exosomes, but also include the production of a variety of both proinflammatory and immuno-suppressive cytokines, as well as the expression of genes with immunoregulatory functions (Ley et al., 2018; Scapini and Cassatella, 2014; Tamassia et al., 2018). Defensive and immune effector functions of neutrophils involve changes in gene expression programs triggered, for example, by ligands for pattern recognition receptors (PRRs) (Ostuni et al., 2016; Tamassia and Cassatella, 2013; Thomas and Schroder, 2013). In recent years, high-throughput sequencing approaches have clarified the interplay between lineage-determining and signal-regulated transcription factors (LDTFs and SRTFs, respectively) in bringing about myeloid-specific gene expression changes in response to various agonists, such as bacterial components and inflammatory cytokines (Glass and Natoli, 2016). Relative to other myeloid cells, such as macrophages and dendritic cells, knowledge on the transcriptional regulatory circuits taking place in human neutrophils under normal conditions and/or upon stimulation, still remains incomplete (Ostuni et al., 2016; Tamassia et al., 2018).

Human neutrophils express and respond to a variety of Toll-like receptors (TLRs), including TLR8, but not TLR7 (Hayashi et al., 2003). In fact, peripheral neutrophils isolated at a purity level greater than 99.7% express only TLR8. However, TLR7 may also give false-positive results if no precautions are undertaken to completely remove all possible contaminating leukocytes from the granulocytes after their isolation from the blood (Gaudreault and Gosselin, 2009; Hayashi et al., 2003; Nagase et al., 2003; Zimmermann et al., 2015, 2016). Consequently, human neutrophils represent an ideal cell model to investigate TLR8-mediated responses specifically. To date, TLR8 ligands, have been shown to trigger or modulate a variety of effector functions of neutrophils, including the survival, the respiratory burst, the phagocytic activities, and the formation of NETs (Thomas and Schroder, 2013). In our research, TLR8 agonists, including R848 and other compounds, such as CL075 or VTX-2337, have

been found to very potently activate expression of multiple inflammatory genes (including interleukin 6 [*IL6*], tumor necrosis factor [*TNF*], *CSF3*, *IL12B*, *IL23A*, *EBI3*, and *CCL23*) and production of the corresponding products (Arruda-Silva et al., 2017; Cassatella et al., 2020; Tamassia et al., 2019; Zimmermann et al., 2015, 2016) by human neutrophils. In particular, we found that the induction of *IL6* gene transcription via TLR8 activation depends on active remodeling of chromatin at the *IL6* genomic locus in human neutrophils, turning it from an "inactive" to an "active" configuration (Zimmermann et al., 2015).

Herein, to characterize the transcriptional circuits associated with activation of human neutrophils globally, as well as to identify transcriptional regulators activated via TLR8 stimulation, we performed whole-transcriptome analysis by RNA sequencing (RNA-seq), as well as by chromatin immunoprecipitation (ChIP) assays, followed by deep sequencing (ChIP-seq) for quantitative measurements at a genome-wide level of histone 3 lysine 27 acetylation (H3K27Ac) and LDTF occupancy. These analyses led to the identification of octamer transcription factor 2/Pit-Oct-Unc 2F2 (OCT2/POU2F2) (POU class 2 homeobox 2) as an unexpected TF involved in the modulation of gene expression in activated neutrophils.

RESULTS

Gene expression profiling in R848-stimulated neutrophils

To understand, on a genomic scale, the transcriptional changes occurring upon TLR8 activation, we performed RNA-seq experiments in neutrophils incubated for 6 and 20 h, with or without 5 μM R848 (Zimmermann et al., 2015). For comparison purposes, RNA-seq experiments were also performed in autologous $CD14^+$ monocytes. We found that the number of genes either up- or downregulated (by a 2-fold difference and adjusted $p < 0.01$) in R848-treated neutrophils were constantly more than 1,000, at both 6 and 20 h of incubation (Figures 1A and S1A). By contrast, although the number of genes modulated by R848 in monocytes was substantially similar to that in neutrophils, more mRNAs were differentially transcribed at 20 h (Figure 1B), but less at 6 h (Figure S1B). Gene Ontology (GO) analysis revealed that the genes upregulated upon treatment with R848 for 20 h associated with pathways related to GO terms involved in the "regulation of innate responses" in neutrophils (Figure 1C) and to the "responses to virus" and "immune processes" in monocytes (Figure 1D).

To identify differentially expressed genes (DEGs) across neutrophils and monocytes incubated with or without R848 for 6 and 20 h, we applied likelihood ratio tests (LRTs) and obtained a total of 9,575 DEGs. Principal-component analysis (PCA) performed on these DEGs indicated that the largest sources of sample variability derive from the intrinsic transcriptional differences characterizing neutrophils and monocytes (namely, PC1), and the treatment with R848 (namely, PC2) (Figure 1E). Surprisingly, the incubation time points (6 or 20 h) were found not to represent a cause of DEG variability (Figure 1E). K-means-clustering analysis of the most variable (top 20%) up/downregulated DEGs identified nine distinct gene clusters (Figure 1F), three of them specifically expressed in neutrophils (i.e., clusters 1–3), four in monocytes (i.e., clusters 4–7), and two in both cell types (i.e., clusters 8–9). Accordingly, cluster 1 was found to include genes constitutively expressed in neutrophils, such as those encoding for their typical markers (*FCGR3B*, *CXCR1*, *CXCR2*, and *CSF3R*) or granule proteins (*ELANE*, *DEFA1B*, *DEFA3*, *LCN2*, and *ARG1*), whereas cluster 2 included genes downregulated by R848, such as *CAT*, *CEACAM4*, *SELL* (CD62L), and *SELPLG* (PSGL-1) (Figure 1F). By contrast, cluster 3 was found to include the genes strongly induced by R848 in neutrophils, such as *PI3* (peptidase inhibitor 3) and *SLPI* (secretory leukocyte peptidase inhibitor), acute phase proteins (such as orosomucoid *ORM1* and *ORM2*), plasminogen activator (*PLAU*), and *CHI3L1* protein (Figure 1F). Interestingly, "neutrophil-mediated immunity" was the most-enriched GO term found as associated with clusters 1, 2, and 3 (Figure S1C). Monocyte-specific clusters 4 and 5 were found to contain, respectively, constitutively expressed genes, such as *VCAN*, *IRF8*, *ANXA2*, *SAMHD1*, and *LGALS1*, and downregulated genes, such as *CSF1R*, *CD36*, and *FCER1A* (Figure 1F; Table S1). Notably, among the most-enriched GO terms associated with clusters 4 and 5, many were related to antigen processing and presentation (Figure S1C), consistent with the ability of monocytes to exert those functions (Jakubzick et al., 2017). Cluster 6 was found enriched for ribonuclear protein mRNAs (Figures 1F and S1C; Table S1), in line with the very efficient translational capacity of monocytes, whereas cluster 7 mainly consisted of R848-induced interferon (IFN)-stimulated genes (ISGs) and, thus, enriched in "defense response to virus" GO terms (Figures 1F and S1C; Table S1). No expression of ISGs was observed in R848-treated neutrophils (as illustrated by Figures 1F and S1D) because they do not upregulate type I IFN expression (Zimmermann et al., 2015, 2016). Furthermore, cluster 7 was found to also include genes encoding for chemokines specifically expressed in monocytes, such as *CCL7*, *CCL8*, and *CCL15*, as well as immunoregulatory cytokines, such as *IL7*, *IL15*, *IL10*, and *IL27* (Figure 1F), the latter two molecules already known as not transcribed in R848-stimulated neutrophils (Cassatella et al., 2020; Zimmermann et al., 2015). Finally, the genes included in clusters 8 and 9 were found to be related to "response to molecule of bacterial origin" GO terms (Figure S1C) and listed many of the cytokines recently shown to be produced by R848-stimulated neutrophils (e.g., *IL6*, *CSF3*, *EBI3*, *IL12B*, *IL23A*, *CCL4*, and *CCL23*) (Cassatella et al., 2020; Tamassia et al., 2019; Tamassia et al., 2018; Zimmermann et al., 2015) other than monocytes. Other cytokine genes emerging from these latter clusters include *CCL1*, *CCL2*, *CCL20*, *CXCL2*, *CXCL3*, *IL1B*, *IL1RN*, *IL36G*, and *TNF* in cluster 8, and *CCL18*, *CCL3*, *CCL3L1*, *CCL4L2*, *CXCL1*, *CXCL8*, *EDN1*, and *OSM* in cluster 9. Notably, R848 was also found to induce, in both cell types, the expression of immunosuppressive molecules, such as *CD274*, *SLAMF7*, and *HHLA2* (clusters 8 and 9) (Figure 1F). In sum, our experiments demonstrate that activation of neutrophils via TLR8 promotes a gene expression program that, at least in part, is remarkably distinct from that of similarly treated autologous monocytes.

Characterization of the genomic response to TLR8 triggering in human neutrophils

To identify the genomic regulatory regions activated via TLR8 engagement and correlate them with the concurrent

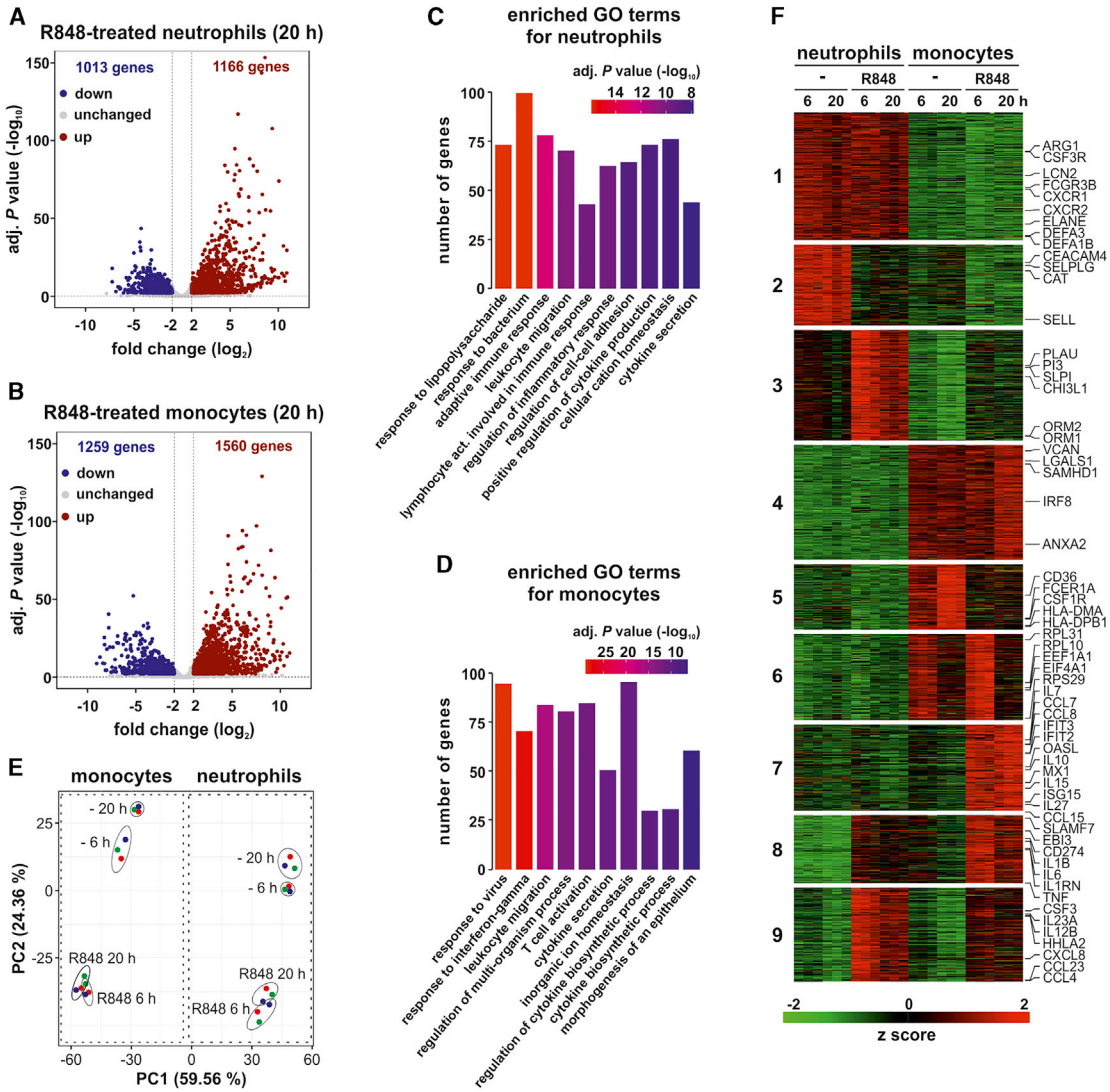

Figure 1. Gene expression profiles of resting and TLR8-activated neutrophils and monocytes

(A and B) Volcano plots displaying the genes differentially expressed in neutrophils (A) and in autologous monocytes (B) incubated with R848 for 20 h. Significantly increased or decreased mRNAs ($p < 0.01$, calculated by Wald's test) are marked by red and blue dots, respectively. Each dot represents the mean value of a transcript from three replicate experiments.

(C and D) Results of enriched Gene Ontology (GO) terms obtained from R848-upregulated genes in neutrophils (C) and monocytes (D) are shown. The top 10 GO-enriched terms, based on p values calculated by hypergeometric distribution, are shown in the bar plots.

(E) PCA scatterplot of differentially expressed genes (DEGs) identified among all samples under investigation (i.e., neutrophils and monocytes incubated with or without R848 for 6 and 20 h). Transcriptomic analysis of cell samples from three different donors (specified by dots of different colors) was performed.

(F) Heatmap of DEGs among neutrophils and monocytes incubated with or without R848 for 6 and 20 h. DEGs were identified by DESeq2, using $p < 0.01$ by LRT, as a selection parameter. Numbers at the left side of the heatmap indicate the nine clusters identified by K-means-clustering analysis. Relative expression levels for a single transcript were calculated by *Z* score.

See also Figure S1 and Table S1

transcriptional changes, neutrophils were incubated for 6 and 20 h with or without R848 (Zimmermann et al., 2015) and then subjected to H3K27Ac ChIP-seq. H3K27Ac marks active genomic *cis*-regulatory elements, including enhancers and promoters, thus enabling the identification of over-represented TF motifs associated with dynamic elements (Ghisletti et al., 2010; Heinz et al., 2010; Mildner et al., 2017; Novakovic et al., 2016; Pham et al., 2012). More than 25,000 H3K27Ac peaks were detectable in neutrophils, regardless of the time point or their activation state (Figure S2A); 2,661 and 2,604 genomic regions (Table S2) gained more than a 2-fold increase in the H3K27Ac levels after, respectively, 6 and 20 h of R848 treatment (Figure 2A), as exemplified by the *CCL3/CCL4* (Figure 2B), *TNF* (Figure 2C), and *IL6* (Figure 2D) loci. By contrast, neutrophils were found to display inaccessible regulatory regions at their *IL10* locus, as evidenced by the

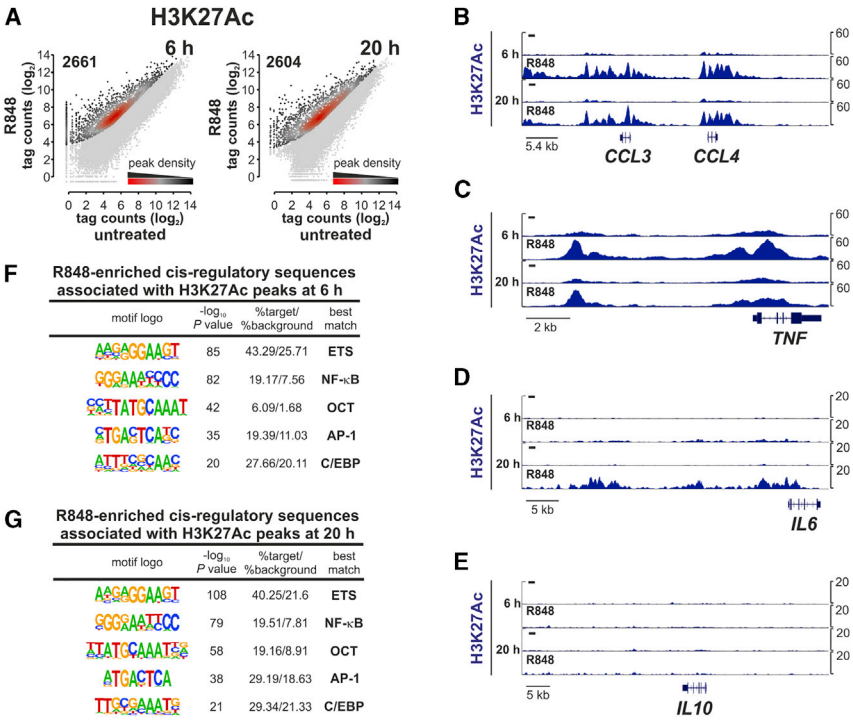

F

R848-enriched cis-regulatory sequences associated with H3K27Ac peaks at 6 h

motif logo	-log10 P value	%target/ %background	best match
	85	43.29/25.71	ETS
	82	19.17/7.56	NF-κB
	42	6.09/1.68	OCT
	35	19.39/11.03	AP-1
	20	27.66/20.11	C/EBP

G

R848-enriched cis-regulatory sequences associated with H3K27Ac peaks at 20 h

motif logo	-log10 P value	%target/ %background	best match
	108	40.25/21.6	ETS
	79	19.51/7.81	NF-κB
	58	19.16/8.91	OCT
	38	29.19/18.63	AP-1
	21	29.34/21.33	C/EBP

Figure 2. Genome-wide profile of the H3K27Ac mark in resting and TLR8-activated neutrophils

(A) Neutrophils were incubated for 6 (left panel) and 20 h (right panel) with 5 μM R848 to perform H3K27Ac ChIP-seq. Peaks with normalized tag counts, which were induced more than 2-fold upon R848-stimulation (numbered in the top-left corners of each panel), are displayed as density plots in the two graphs. The color for each dot in the density plots stands for the relative number of the peaks, according to the bar placed at the right bottom corner of each graph (n = 2).

(B–E) Representative snapshots of H3K27Ac ChIP-seq in human neutrophils incubated with or without R848 for 6 and 20 h, illustrating the *CCL3-CCL4* (B), *TNF* (C), *IL6* (D), and *IL10* (E) genomic loci.

(F and G) Tables list the sequence logos corresponding to the enriched sequence elements found by *de novo* motif-discovery analysis, using a random GC-corrected genomic background, of nucleosome-free regions (NFRs) in R848-induced peaks obtained from H3K27Ac ChIP-seq at 6 h (F) and 20 h (G). For each motif logo, tables display the enrichment p value ($-\log_{10}$) for the motif over-representation; the percentage of the target versus the background sequences, containing the motif; and the name of the TF family corresponding to the best-matched motif.

See also Figure S2 and Table S2.

absence of the H3K27Ac histone mark, confirming previous observations by ChIP-qPCR (Tamassia et al., 2013) (Figure 2E). Such a chromatin conformation, in fact, prevents the binding of TFs activated by TLR ligands, thereby precluding any transcription. We also found that the loci encoding R848-upregulated mRNAs were significantly marked by H3K27Ac deposition (Figure S2B), consistent with the notion that H3K27Ac strictly correlates with increased expression of nearby genes (Cotney et al., 2012; Kundaje et al., 2015).

Subsequent *de novo* motif discovery analysis of R848-induced H3K27Ac peaks revealed a significant enrichment of motifs associated with SRTFs, including members of the nuclear factor κB (NF-κB) and activator protein 1 (AP-1) families (Figures 2F and 2G). It also uncovered consensus motifs associated with well-known myeloid LDTFs, such as E26 transformation-specific (ETS) and CCAAT/enhancer-binding protein (C/EBP) family members (Figures 2F and 2G). Notably, a significant enrichment of a motif related to the OCT/POU family of transcription factors, namely 5′-ATGCAAAT-3’ (Malik et al., 2018; Zhao, 2013), was also identified in neutrophils incubated with R848 and more evident after 20 h than 6 h of stimulation (Figures 2F and 2G).

PU.1 and C/EBPβ bind to enhancers present in TLR8-activated elements

To corroborate and extend the results obtained by the H3K27Ac ChIP-seq, we performed additional ChIP-seq experiments targeting PU.1 and C/EBPβ in neutrophils incubated for 20 h with or without R848. PU.1 and C/EBPβ were chosen among the various TFs that can bind to ETS and C/EBP motifs because PU.1 is critical for establishing and, in turn, maintaining, cell-type-specific repertoires of enhancers and promoters in myeloid cells (Ghisletti et al., 2010; Heinz et al., 2010), whereas C/EBPβ is the most highly expressed C/EBP family member in mature neutrophils (Cloutier et al., 2009; Häger et al., 2010). By doing so, we identified 26,381 and 15,990 genomic sites to which PU.1 and C/EBPβ were bound in resting neutrophils, respectively (Figures S2C and S2D). PU.1- and C/EBPβ-binding sites increased to 31,909 and 22,857 in R848-treated cells, respectively (Figures S2C and S2D). Remarkably, in neutrophils incubated with R848 for 20 h, the increased recruitment of both PU.1 and C/EBPβ was associated with most of the 2,604 genomic regions with enhanced H3K27Ac (Figure 3A). That finding further demonstrates that both PU.1 and C/EBPβ are involved in the *de novo* assembly of active regulatory regions in TLR8-activated neutrophils.

To better investigate the genomic regulatory regions that, upon stimulation, are characterized by enriched PU.1- and C/EBPβ binding, we restricted our analysis to the LDTF peaks that were induced at least 2-fold by R848. As a result, we detected 3,818 PU.1 peaks and 5,474 C/EBPβ peaks induced by R848 treatment (Figures 3B and 3C; Table S3), which, for both LDTFs, were closely associated with genes whose expression was significantly increased by TLR8 stimulation (Figures 3D and 3E). *De novo* motif-discovery analysis of regions surrounding R848-inducible PU.1- or C/EBPβ-binding sites (±100 bp from the summit peaks) was used to identify the most-common sequence elements. As expected, the canonical ETS and C/EBP motifs were significantly more enriched in regions containing R848-induced PU.1- and C/EBPβ-binding peaks from PU.1 and C/EBPβ ChIP-seq, respectively (Figures 3F and 3G). The other motifs found as highly enriched in these regions were, again, those for the OCT family, in addition to NF-κB and AP-1 (Figures 3F

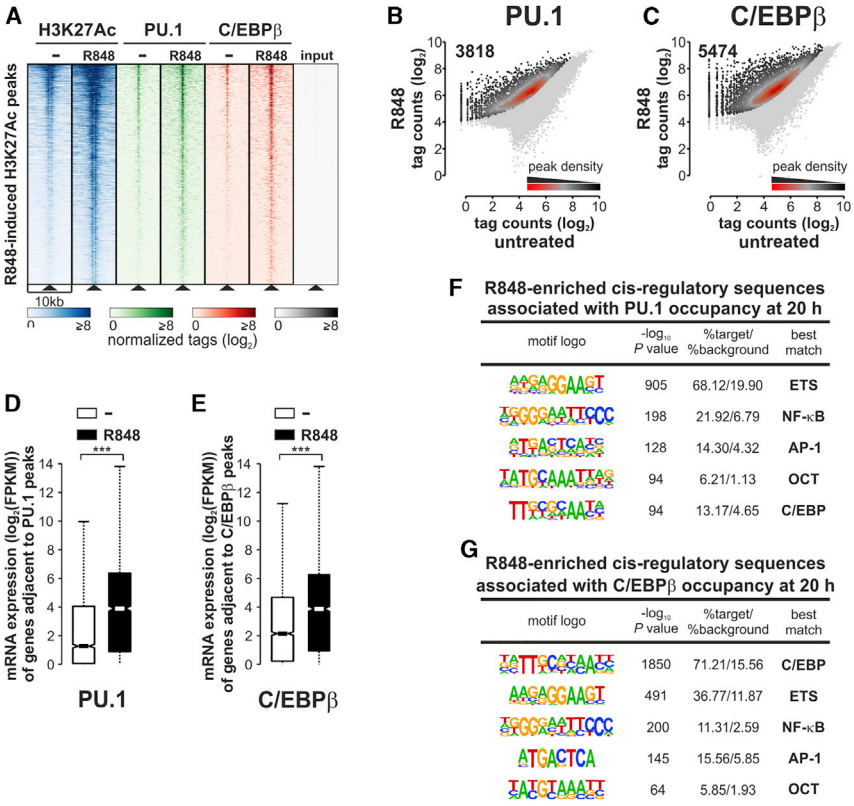

Figure 3. Characterization of TLR8-induced PU.1- and C/EBPβ-binding regions

(A) Heatmaps of 6-kb-wide regions from ChIP-seq profiles of H3K27Ac, PU.1, and C/EBPβ made in resting and TLR8-stimulated neutrophils and centered on R848-induced H3K27Ac NFRs. Representative experiment, n = 2.

(B and C) Neutrophils were incubated for 20 h with R848 to perform PU.1 (B) and C/EBPβ (C) ChIP-seq. Peaks were then displayed as described in the legend to Figure 2A.

(D and E) Boxplots showing the distribution of mRNA expression levels (as $\log_2$ fragments per kilobase of transcript per million mapped reads [FPKM]) for genes adjacent to R848-induced PU.1 (D) and C/EBPβ (E) peaks. Asterisks stand for a significant increase in the mRNA expression levels of genes associated with R848-induced peaks (***$p < 0.001$ by Wilcoxon signed-rank test).

(F and G) Tables list the sequence logos corresponding to enriched sequence elements found by *de novo* motif-discovery analysis of R848-induced peaks obtained from PU.1 (F) and C/EBPβ (G) ChIP-seq, as explained in the legend to Figures 2F and 2G.

See also Figure S2 and Table S3.

and 3G). Thus, as observed for H3K27Ac ChIP-seq (Figures 2F and 2G), OCT motifs were also enriched at the R848-induced PU.1 and C/EBPβ peaks, together with the NF-κB and AP-1 motifs. Finally, we analyzed the distribution of the genomic distance between *de novo* enriched motifs, precisely, ETS, C/EBP, NF-κB, AP-1, and OCT and R848-induced PU.1 and C/EBPβ peaks (Figures 3F and 3G). Such analysis clearly shows that NF-κB, AP-1, and OCT motifs result in close proximity to R848-induced PU.1 and C/EBPβ peaks, being positioned within 300 bp from the center of their peaks (Figures S2E). Data, therefore, suggest that, in activated neutrophils, the genomic loci characterized by PU.1 or C/EBPβ deposition function as regulatory regions for the recruitment of other TFs.

OCT2 as a TF-modulating gene expression in TLR8-activated neutrophils

The octamer (5′-ATGCAAAT-3′) motif identified by H3K27Ac, PU.1, and C/EBPβ ChIP-seq (Figures 2F, 2G, 3F, and 3G) is specifically recognized by a highly conserved group of TFs composed of eight members, known as OCTs, and belonging to the larger family of POU domain factors (Malik et al., 2018; Zhao, 2013). We found that, among OCTs, resting neutrophils express *POU2F2*/*OCT2* and *POU2F1*/*OCT1* mRNA (Figure 4A). However, different from *OCT1*, *OCT2* transcripts were induced with slow kinetics upon R848 treatment, reaching high levels after 20 h of stimulation (Figure 4B). Consistently, OCT2, but not OCT1 (data not shown), protein was found to be almost absent in untreated neutrophils but detectable after stimulation with R848 for 6 h, with high expression after 20 h (Figure 4C), and exclusively localized in the nuclei (Figure S3A). Other neutrophil agonists, including lipopolysaccharide (LPS) and TNF-α, but not granulocyte colony stimulating factor (G-CSF), were found able to induce *OCT2* mRNA (Figure 4D) and protein (Figure 4E) but at lower levels than either R848 or VTX-2337 (Figures 4D and 4E), the latter a more-selective ligand for TLR8 (Lu et al., 2012).

To analyze the genomic distribution of OCT2, we performed ChIP-seq experiments in neutrophils incubated for 20 h with or without R848. We could identify only 83 significantly conserved peaks in resting cells (Figure 4F), which dramatically augmented (9,287) in response to R848 (Figure 4F). OCT2 binding was observed, for instance, at the *IRAK3* (+7.7 kb from transcription start site [TSS]), *LYN* (+50.8 kb from TSS), and *MAP3K8* (+139 kb from TSS) genomic loci (Figure 4G), as also confirmed by ChIP-qPCR experiments performed in neutrophils incubated with VTX-2337, LPS, or TNF-α (Figure 4H). In this case, *IRAK3*, *LYN*, and *MAP3K8* genomic loci were selected for their content of OCT consensus motif and high levels of H3K27Ac and PU.1 peaks induced by TLR8. Of note, the TLR8-specific ligand VTX-2337 was found to induce a neutrophil response equivalent to that triggered by R848 in terms of upregulation of *OCT2* mRNA (Figures 4D) and protein (data not shown), as well as activation of OCT2 (Figure 4H). On the other hand, CU-CPT9a, a TLR8-specific inhibitor (Zhang et al., 2018), completely blocked R848- but not LPS-induced *OCT2* and *CXCL8* mRNA expression (data not shown), once again, supporting the notion that, in human neutrophils, R848 exclusively signals through TLR8. In line with the very low levels of *OCT1* mRNA expression (Figure 4A), ChIP-qPCR did not reveal any binding of OCT1 at the *IRAK3* and *LYN* genomic

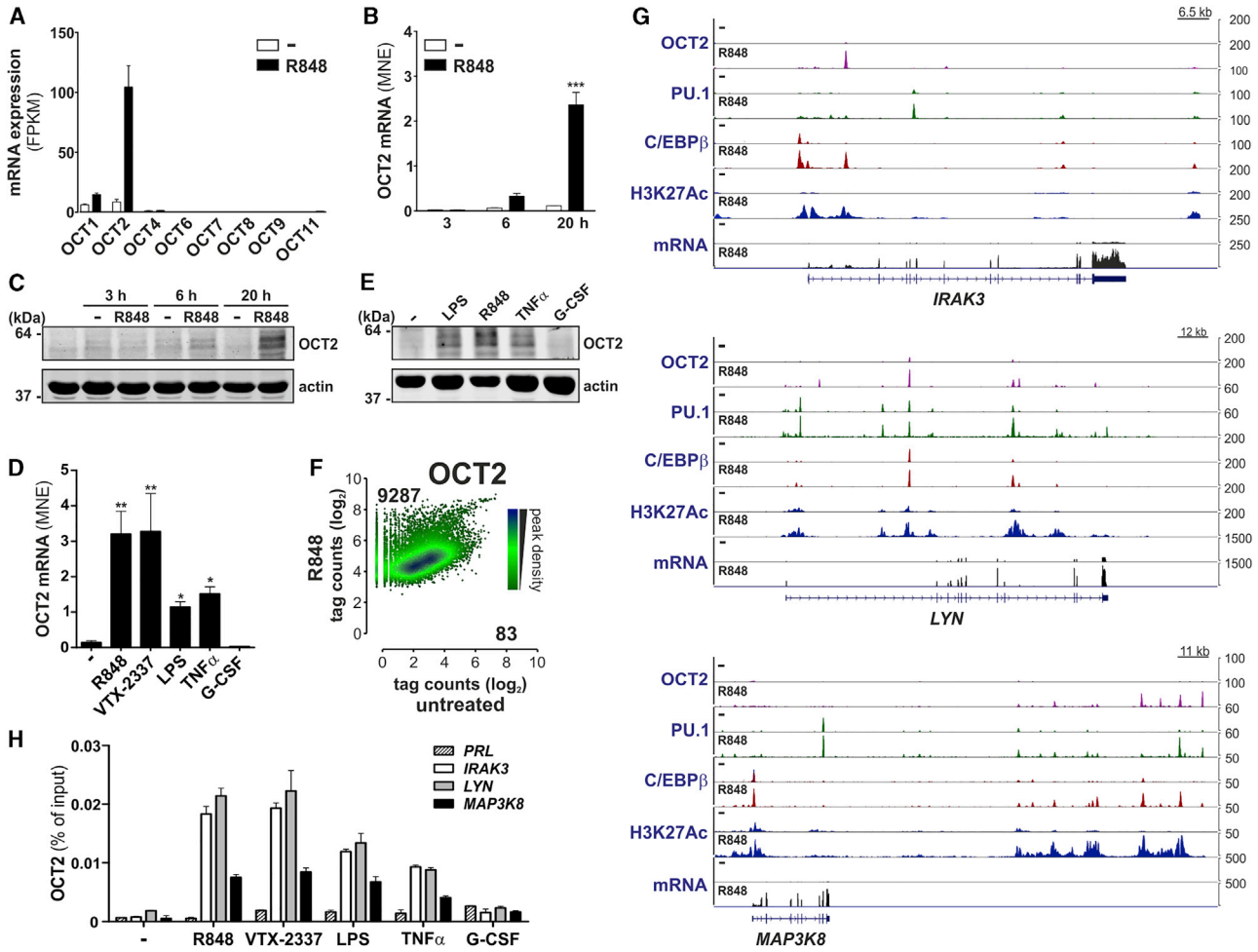

Figure 4. OCT2 induction and activation in neutrophils treated with R848 or other pro-inflammatory agonists

(A) OCT family genes expressed in neutrophils incubated with or without R848 for 20 h, based on RNA-seq analysis.

(B and D) *OCT2* mRNA expression in neutrophils cultured (B) for up to 20 h with R848 (n = 3–9); and (D) for 20 h with 5 μM R848, 1 μM VTX-2337, 1 μg/mL LPS, 10 ng/ml TNF-α, and 1,000 U/mL G-CSF (n = 3). Gene expression is depicted as mean normalized expression (MNE) units after normalization to GAPDH mRNA (mean ± SEM). Asterisks stand for significance [*p < 0.05, **p < 0.01, ***p < 0.001, by two-way ANOVA followed by Bonferroni's post test for (B) or by one-way ANOVA followed by Tukey's post test for (D)].

(C and E) OCT2 immunoblotting of neutrophils, either untreated or incubated: (C) for 3, 6, and 20 h with R848 (representative experiment, n = 3); or (E) for 20 h with 5 μM R848, 1 μg/mL LPS, 10 ng/mL TNF-α, and 1,000 U/mL G-CSF (representative experiment, n = 3).

(F) Neutrophils were incubated for 20 h with R848 to perform OCT2 ChIP-seq. Peaks in untreated (x axis) and R848-stimulated (y axis) neutrophils are displayed as density plots. The color for each dot in the density plots stands for the relative number of the peaks according to the bar placed at the right side of the graph. The number of sites identified in resting and TLR8-activated neutrophils is indicated at the lower-right and the upper-left corners of the plot, respectively.

(G) Genomic snapshots showing OCT2, PU.1, C/EBPβ, and H3K27Ac peaks, as well as *IRAK3*, *LYN*, and *MAP3K8* gene expression levels, in neutrophils incubated with R848 for 20 h.

(H) OCT2 ChIP-qPCR assays made in neutrophils, cultured in the presence or absence of 5 μM R848, 1 μM VTX-2337, 1 μg/mL LPS, 10 ng/mL TNF-α, and 1,000 U/mL G-CSF for 20 h to evaluate the recruitment of OCT2 to the genomic loci of *IRAK3* (+7.7 kb from TSS), *LYN* (+ 51 kb from TSS), *MAP3K8* (+139 kb from TSS), and *PRL* (promoter). Co-immunoprecipitated DNA is expressed as a percentage of the input ± SD (n = 2).

See also Figure S3 and Table S3.

loci, in either resting or R848-treated neutrophils, unlike what was observed in Daudi cells (Figure S3B). Consistent with the increment of OCT2-binding sites in TLR8-activated neutrophils, the number of genes associated with more than one OCT2-binding site in stimulated cells was strongly increased (Figure S3C). Moreover, the density of OCT2-binding to the enhancer regions was substantially increased as a result of TLR8 engagement (Figure S4A), in line with the H3K27Ac peaks. However, under both resting and R848-stimulatory conditions, the percentage of peaks located at the promoter regions was greater in OCT2 than it was in PU.1 or C/EBPβ ChIP-seq datasets (Figures S4A–S4C).

Given that OCT2 is known to have important roles in the development and function of B lymphocytes (Hodson et al., 2016), we compared OCT2 genomic occupancy in resting/R848-treated

neutrophils versus the GM12878 lymphoblastoid B cell line (Kundaje et al., 2015). The OCT2-recognition motif retrieved from the *de novo* motif discovery was identical in both cell types, indicating that the motif itself does not contribute to cell-specific binding patterns (Figure S4D). However, we found that the peaks in common between the GM12878 cells and R848-treated neutrophils were few (2,904) (Figure S4E). Similar findings were also observed when examining PU.1 ChIP-seq in GM12878 and R848-treated neutrophils (Figure S4F). Data indicate that OCT2 and PU.1, are bound to different and cell-specific sites, suggesting that they presumably regulate the expression of different genes in human neutrophils and B cells.

Consistent with the dramatic increase of OCT2 protein in R848-treated neutrophils (Figure 4C), the number of OCT2 peaks that were induced at least 2-fold by R848 was found very high (namely, 4,401; Figure 5A; Table S3) similar to what was observed for PU.1 and C/EBPβ (Figures 3B and 3C). Remarkably, genomic sites exhibiting R848-induced OCT2 binding also displayed a concomitant increment of PU.1 and C/EBPβ binding, as well as increased H3K27Ac levels (Figure 5B). In line with the H3K27Ac increment, expression levels of the genes proximal to the OCT2-induced peaks were significantly increased by TLR8 stimulation (Figure 5C). Data indicate that a group of regulatory regions that displayed increased OCT2 deposition and are co-occupied by increased levels of PU.1 and C/EBPβ emerge in R848-treated neutrophils. Demonstrative genomic loci characterized by co-occupation of these three TFs consist of enhancer and promoter regions of many cytokine genes, such as *CCL3/CCL4*, *IL6*, *TNF*, *CXCL8*, *IL1A/IL1B*, *IL12B*, and *IL23A* (Figure S5). Interestingly, OCT2-induced peaks revealed significant co-enrichment of motifs related to PU.1 and C/EBP (Figure 5D), in addition to OCT itself (Figure 5D), confirming previous data obtained by PU.1 and C/EBPβ ChIP-seq (Figures 3F and 3G). In addition, the OCT2-induced motif signature also contained NF-κB (8.26%) and AP-1 (12.55%) sequence motifs (Figure 5D), as previously identified in the R848-induced PU.1- and C/EBPβ-binding sites. Analysis with the genomic regions enrichment of annotation tool (GREAT) (McLean et al., 2010), performed to identify functional specificities associated with the TLR8-dependent, induced OCT2 peaks, demonstrated that OCT2 peaks are strongly associated with several ontology terms related to the immune responses (as biological process) as well as to viral infection and autoimmune diseases (as disease ontology) (Figure 5E). Therefore, these results are consistent with the presumed biological role of TLR8 (Vierbuchen et al., 2019).

To identify candidate OCT2-target genes, we used the binding and expression target analysis (BETA) tool, which integrates ChIP-seq with differential gene-expression data (Wang et al., 2013). Accordingly, BETA first assigned an OCT2 regulatory potential (RP) score to each gene, based on two criteria: (1), the number of OCT2-binding sites within ±100 kb from the TSS for each queried gene; and (2), the distance between these OCT2-binding sites and the related TSS. Then, BETA combines the OCT2 RP scores with mRNA expression differences to produce a p-value-like score, indicating the likelihood of it being a real, direct target gene of the TF. Moreover, BETA runs a statistical test to categorize whether a given TF functions as a repressor, activator, or both. We found a strong association between upregulated genes and OCT2-binding sites (Kolmogorov-Smirnov test, $p = 8.86 \times 10^{-57}$; Figure 5F), suggesting that many of these R848-upregulated genes might represent direct targets of OCT2. By contrast, a modest association was observed between OCT2 binding and R848-mediated transcriptional downregulation (Figure 5F), a finding that likely reflects a primary role for OCT2 in transcriptional activation, rather than in repression. Interestingly, among the genes characterized by a high potential regulatory score (as determined by BETA), in addition to many genes encoding for cytokines such as *CCL3*, *CCL4*, *IL1B*, *IL12B*, and *IL6*, emerged *NFKBIZ*, a gene that exhibits crucial immunomodulatory functions (Yamamoto et al., 2004), and *CD274*, an immune inhibitory receptor ligand, which suppresses anti-tumor T-cell-mediated immune responses (Table S4).

OCT2 binds to both common and cell-specific genomic regions in R848-treated neutrophils and monocytes

We then investigated the effect of R848 on the expression and function of OCT2 in human monocytes. Similar to what was observed in neutrophils, OCT2 also represents the most expressed member of the OCT family in monocytes, in which R848 increases its transcription as well (Figure S6A). At the protein level, monocytes constitutively express detectable amounts of OCT2 (Figure S6B), confirming previous studies (Neumann et al., 2000). Treatment of monocytes with R848 was found to maintain constitutively elevated OCT2 protein levels, which would otherwise decrease upon cell culture (Figure S6B). By performing ChIP-seq experiments under the same experimental conditions used for autologous neutrophils, we could identify 1158 OCT2 peaks in monocytes incubated for 20 h in culture medium (Figure S6C), which increased to 6,881 upon R848-treatment (Figure S6C); 4,531 of which at levels 2-fold higher than that in resting cells (Figure S6D; Table S5). The greater number of OCT2 peaks observed in resting monocytes than in resting neutrophils is in line with the greater expression of OCT2 protein in monocytes (Figures 4C, 4F, S6B, and S6C). *De novo* motif-discovery analysis of the R848-induced 4,531 OCT2 peaks in the monocytes revealed significant co-enrichment of OCT2 itself and ETS, C/EBP, NF-κB, and AP-1 related motifs (Figure S6E), as in R848-treated neutrophils (Figure 5D). Of note, the AP-1 motif was found as much more enriched in R848-induced OCT2 peaks of monocytes (Figure S6E) than it was in neutrophils (Figure 5D), even though, in the latter cells, AP-1 enrichment was found significant. In addition, for monocytes, the binding motif for OCT2 was almost identical to that obtained from analyzing neutrophils and GM12878 cells (Figure S4D). On the other hand, analysis of the OCT2-induced peaks in monocytes and autologous neutrophils uncovered that some of them (3,404) were located in the same genomic regions, whereas others were more specific, either for neutrophils (1,545) or for monocytes (2,463) (Figures 6A and 6B). Examples of common, neutrophil-, and monocyte-specific OCT2 peaks were found at the genomic locus of *IL1B*, *PLEK*, and *ITGB8*, respectively (Figure 6B). Consistently, expression levels of the genes proximal to neutrophil- or monocyte-specific OCT2 peaks were significantly higher in the corresponding R848-stimulated cell type than in the other one (Figure 6C). Taken together, our data prove that OCT2 is induced in both neutrophils and monocytes

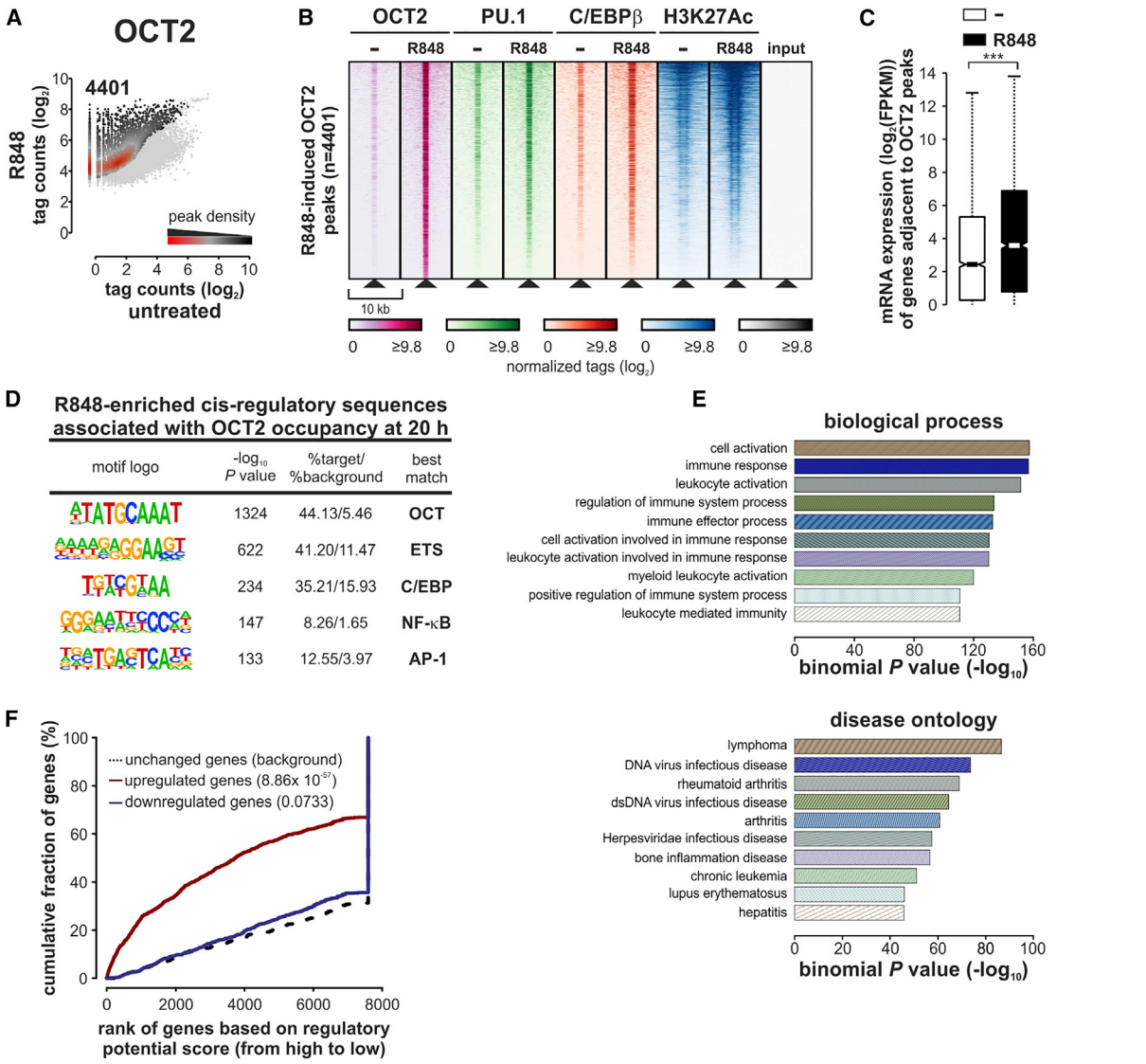

Figure 5. Characterization of OCT2-binding regions in R848-treated neutrophils

(A) Neutrophils were incubated for 20 h with R848 to perform OCT2 ChIP-seq. Peaks were then displayed as described in the legend to Figure 2A.

(B) Heatmaps of 6-kb-wide regions from ChIP-seq profiles of H3K27Ac, PU.1, C/EBPβ, and OCT2 made in resting and TLR8-stimulated neutrophils and centered on R848-induced OCT2 peaks. Representative experiment, n = 2

(C) Boxplots showing the distribution of mRNA expression levels (as $\log_2$ FPKM) for genes adjacent to R848-induced OCT2 peaks. Asterisks stand for a significant increase in the mRNA expression levels of genes associated with R848-induced peaks (***$p < 0.001$ by Wilcoxon signed-rank test).

(D) Tables list the sequence logos corresponding to enriched sequence elements found by *de novo* motif-discovery analysis (using a random GC-corrected genomic background) of R848-induced peaks obtained from OCT2 ChIP-seq, as explained in the legend to Figures 2F and 2G.

(E) Functional annotation of R848-induced OCT2 peaks performed using GREAT. The top over-represented categories belonging to "biological process" (top panel) and "disease ontology" (bottom panel) are shown. The x axis values (depicted in logarithmic scale) correspond to the binomial p value calculated by GREAT.

(F) Integration of RNA-seq and ChIP-seq data to determine whether OCT2 exerts activatory or repressive functions. Upregulated (red) and downregulated (blue) genes are plotted with respect to the non-affected genes as background (dashed line). Genes are cumulated by the rank based on the regulatory potential score. See also Figures S4 and S5 and Tables S3 and S4.

incubated with R848 and that it binds to both common and cell-specific genomic regions. Therefore, it is plausible to speculate that OCT2 contributes to conditioning the different gene-expression programs observed in neutrophils and monocytes incubated with R848.

Downregulation of inflammatory genes in OCT2-silenced granulocytic HL-60 cells

To formally determine how OCT2 affects gene expression, given that OCT2 depletion cannot be achieved in primary neutrophils (because of their fragility and refractoriness to genetic

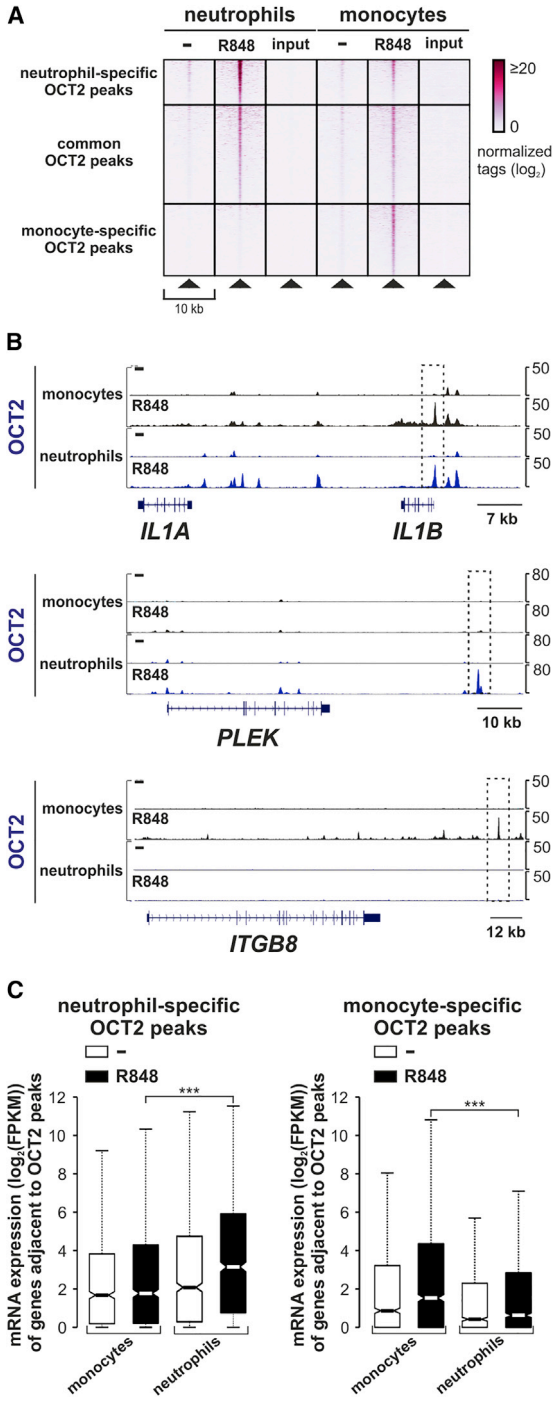

Figure 6. Comparison between the OCT2 peaks induced by R848 in neutrophils and monocytes

(A) Heatmaps of 6-kb-wide regions from ChIP-seq profiles of OCT2 performed in resting and TLR8-stimulated neutrophils and monocytes (representative experiment, n = 2).

(B) Genomic snapshots of neutrophils and monocytes incubated with or without R848 for 20 h, showing examples of OCT2 peaks in common (*IL1A-IL1B*) and in neutrophil-specific (*PLEK*) and monocyte-specific (*ITGB8*) genomic loci.

(C) Boxplots showing the distribution of mRNA expression levels (as $\log_2$ FPKM) for genes adjacent to neutrophil-specific (left panel) or monocyte-specific (right panel) OCT2 peaks. Asterisks stand for significant differences in the mRNA expression levels of genes associated with R848-induced peaks between neutrophils and monocytes (***p < 0.001 by Wilcoxon signed-rank test).

See also Figures S6 and Tables S3, S4, and S5

manipulation), we tried to deplete OCT-2 in hematopoietic stem cells (HSCs) differentiated *in vitro* to neutrophils. In fact, HSCs, cultured with a specific G-CSF-containing cytokine cocktail, mature fully into neutrophils and respond appropriately to TLR8 agonists (data not shown). However, when genetically modified by nucleofection, HSCs inexorably die after maturation to neutrophils. We, thus, performed OCT2 depletion in HL-60 cells differentiated into neutrophil-like cells by DMSO, which represents a surrogate, well-accepted cell model of mature neutrophils (Collins et al., 1978; Tamassia et al., 2007), which has the additional advantage of allowing reliable transfections (Ear and McDonald, 2008). Accordingly, DMSO-treated HL-60 cells were found to respond to R848 similarly to human neutrophils in terms of *OCT2*, *NFKBIZ*, *CXCL8*, *TNF*, *CCL3*, *CCL4*, *IL6*, *IRAK3*, and *LYN* mRNA induction (Figure 7A), albeit with more accelerated kinetics. The latter phenomenon might be explained by the fact that HL-60 cells display much more efficient transcriptional machinery than do mature neutrophils, as also proven by their greater RNA content per cell than that found in neutrophils (data not shown). Moreover, in DMSO-treated HL-60 cells, OCT2 protein was already induced by R848 at high levels after 6 h, even though its expression was found strongly decreased by specific OCT2 silencing (Figure 7B). Notably, antigenic OCT2 detected in DMSO-treated HL-60 cells appears identical to OCT2 present in control cells (Raji and Daudi B cell lines in this case; Figure S6F) and, therefore, comparable to antigenic OCT2 detected in activated neutrophils (Figures 4C and 4E). However, transcriptome analysis revealed that, in mock-transfected granulocytic HL-60 cells, the number of genes significantly upregulated by R848 was 625, whereas small interfering RNA (si)-OCT2-treated cells it decreased to 559. Under the latter experimental conditions, 265 genes were inhibited by more than 20%, at the expression level, as compared with that of the si-control (si-CTRL), whereas 26 genes were, instead, enhanced (Figure 7C). Among the downregulated genes, *CXCL8*, *NFKBIZ*, *IL-1β*, *IRAK3*, *LYN*, and many others were found (Figure 7C; Table S6), in addition to (as expected) OCT2. These results were then validated by qRT-PCR, which confirmed that, although OCT2 silencing significantly reduces the induction of *CXCL8*, *NFKBIZ*, and *IRAK3* mRNAs by R848, it increases that of *PHLDB1* and *ADAMDEC1* (Figure 7D). Importantly, most OCT2-dependent genes induced by R848 in DMSO-treated HL-60 cells (n = 265) also displayed OCT2-binding sites in R848-treated neutrophils (n = 140), at either their promoter or enhancer regions. We also performed gene set enrichment analysis (GSEA) on OCT2-target genes identified by BETA analysis in human neutrophils and found that their distribution in the R848-treated granulocytic HL-60 cell datasets correlated with the genes down-modulated by OCT2 knockdown (false-discover rate [FDR] < 0.05) (Figure 7E).

In sum, data obtained from OCT2-silenced granulocytic HL-60 cells are in accordance with what was inferred by BETA analysis in human neutrophils, altogether pointing to OCT2 as a TF mainly exerting a role of transcription amplifier in TLR8-activated neutrophils.

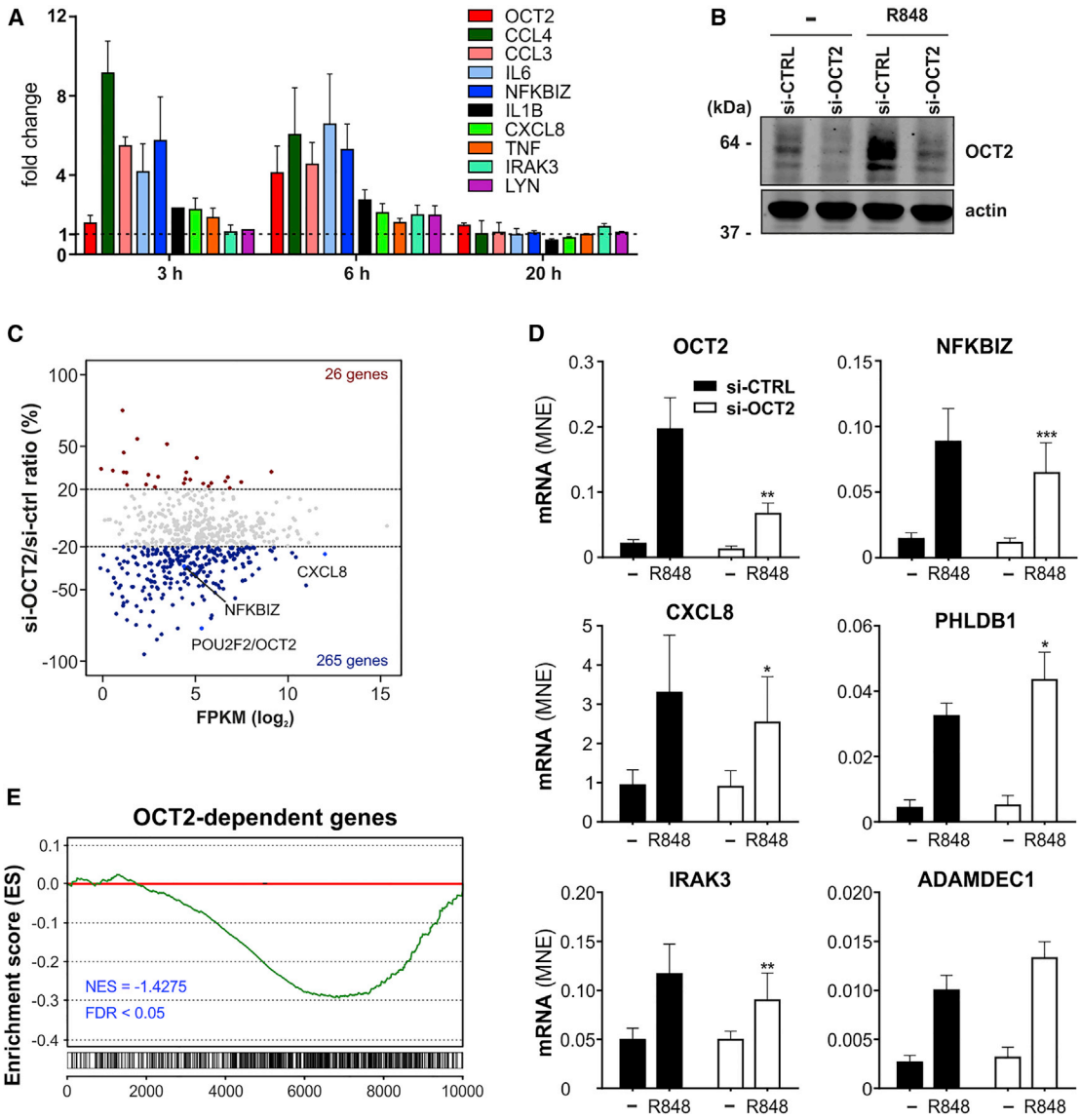

Figure 7. Silencing of OCT2 in HL-60 cells differentiated to neutrophils

(A) mRNA expression profiles for *OCT2*, *CCL3*, *CCL4*, *IL6*, *NFKBIZ*, *CXCL8*, *TNF*, *IRAK3*, *LYN*, and *IL1B* in DMSO-differentiated HL-60 cells incubated with R848 for the times indicated. Results are expressed as fold induction of mRNA levels (mean ± SD, n = 3).

(B–E) DMSO-differentiated HL-60 cells were transfected by nucleofection with si-CTRL or si-OCT2 and then stimulated with R848 for 6 h.

(B) OCT2 protein levels in si-CTRL or si-OCT2 cells by immunoblotting.

(C) Scatterplot comparing the mRNA expression levels of genes upregulated by R848 in granulocytic HL-60 (as FPKM $\log_2$, x axis) versus the ratio of mRNA expression between R848-stimulated si-OCT2 and si-CTRL granulocytic HL-60 (as a percentage, y axis). The genes whose expression is increased or decreased by si-OCT2 transfection more than 20% are marked by red and blue dots, respectively. Values were calculated from four independent experiments.

(D) Validation of *OCT2*, *NFKBIZ*, *CXCL8*, *IRAK3*, *PHLDB1*, and *ADAMDEC1* mRNA expression by qRT-PCR (n = 4). Gene expression is depicted as MNE units after normalization to GAPDH mRNA (mean ± SEM). Asterisks stand for significance (*p < 0.05, **p < 0.01, ***p < 0.001, by two-way analysis of variance followed by Bonferroni's post test).

(E) GSEA of the relationship between differentially expressed genes in si-OCT2 versus si-CTRL R848-stimulated granulocytic HL-60 cells and putative OCT2 target genes identified in R848-treated human neutrophils by BETA. Note that the enrichment is significantly higher (FDR < 0.05) in genes downregulated by si-OCT2 treatment, as revealed by the negative normalized enrichment score (NES).

See also Figures S6 and Tables S6

DISCUSSION

TLR8 is known to act as an endosomal, PRR-recognizing, guanosine- and uridine-rich sequence of single-stranded RNA (ssRNA) viruses, including influenza viruses, HIV-1, vesicular stomatitis virus (VSV), Sendai virus, coxsackie B virus, flaviviruses, and coronaviruses, including SARS-CoV-2 (Lester and Li, 2014). Moreover, recent studies have identified that recognition of

microbial viability by human monocytes, via TLR8-mediated identification of bacterial RNA, acts as a potent stimulus for follicular helper T cell differentiation and vaccine responses (Ugolini et al., 2018). In that context, TLR8 ligands, such as R848/resquimod, VTX-2337/motolimod, and 3M052, are currently catching great interest for therapeutic applications. These molecules have been reported to exert potent adjuvant activities for their ability to induce robust, antigen-specific, humoral- and Th1-immune responses (Temizoz et al., 2018). Consequently, several clinical trials are currently ongoing to test the efficacy of TLR7/TLR8 ligands, either alone or in combination with monoclonal antibodies or chemotherapeutic agents, for the treatment of cancer or as adjuvants for vaccines (Chi et al., 2017). Our laboratory has recently demonstrated that R848, CL075 (Arruda-Silva et al., 2017; Zimmermann et al., 2015; Zimmermann et al., 2016), and VTX-2337 (Cassatella et al., 2020) act as very potent activators of human neutrophils, particularly for the production of proinflammatory cytokines. However, although important for a better comprehension of the activities of these drugs at a systemic level, accurate analysis of the transcriptional response of neutrophils to TLR8 ligands and its related molecular regulation has not yet been performed.

In this study, we report that, when incubated with R848, human neutrophils modify their global transcriptome at levels quantitatively similar to those observed in monocytes, which are cells traditionally known as very transcriptionally active (Guilliams et al., 2018). Most genes induced in neutrophils by R848 were found related to the inflammatory response, as expected. Nonetheless, many R848-induced genes encode for molecules displaying immunosuppressive functions. These data might be important in the context of COVID-19 pathogenesis, for which the contribution of neutrophils is under investigation (Nathan, 2020). SARS-CoV-2 possesses, in fact, more ssRNA fragments recognizable by TLR7/8 than other coronaviruses have (Moreno-Eutimio et al., 2020), which may presumably target and, consequently, activate myeloid cells, including neutrophils and monocytes. If so, on the one hand, neutrophils might contribute to the so-called cytokine storm syndrome observed in patients infected by SARS-CoV-2 (Li et al., 2020), or, on the other hand, neutrophils might act as immunosuppressive cells.

To identify putative, still-unknown TFs involved in such a transcriptional response, we performed genome-wide measurements of H3K27Ac deposition and then *de novo* motif analysis of the genomic regions underneath TLR8-increased H3K27Ac peaks. As a result, we observed a significant enrichment of consensus motifs corresponding to LDTFs known to be involved in myeloid differentiation (Ostuni et al., 2016) and chromatin remodeling (Kaikkonen et al., 2013; Ostuni et al., 2013), namely, to ETS and C/EBP family members. Because PU.1 (an ETS member) is known to be essential for the normal maturation and function of neutrophils (Anderson et al., 1998; Fischer et al., 2019), whereas C/EBPβ represents the most-expressed C/EBP family member in mature neutrophils (Cloutier et al., 2009); in which, it has been shown to control cytokine induction (Cloutier et al., 2009), and we subsequently performed PU.1 and C/EBPβ ChIP-seq. The latter experiments uncovered a wide distribution of PU.1 and C/EBPβ across all neutrophil genome, including in key genes involved in the inflammatory response, in accordance with their LDTF role. Moreover, PU.1 and, at a higher degree, C/EBPβ, were profoundly redistributed in neutrophils treated with R848, once again confirming that, after activation, neutrophils undergo major modifications at the chromatin level, in turn, resulting in marked transcriptional changes. Similar results for PU.1 were described to occur in murine neutrophils derived from *in-vitro*-differentiated bone marrow (BM) progenitors and then stimulated with *Candida albicans* (Fischer et al., 2019). However, ablation experiments also uncovered that, intriguingly, PU.1 reduces the accessibility of enhancers via histone deacetylase 1 (HDAC1) recruitment to specific immune-related genes, ultimately displaying an inhibitory role on transcription (Fischer et al., 2019). We could not address this latter effect of PU.1 in our system because, in the absence of stimulation, OCT2 is not expressed. Moreover, by genome-wide chromosome conformation capture approach (HiC), human neutrophils have recently been demonstrated to undergo large-scale alterations in chromatin organization upon exposure to *Escherichia coli* or Phorbol 12-Myristate 13-Acetate (PMA) (Denholtz et al., 2020). In particular, cytokine and other immune-response genes have been shown to gain euchromatic features upon neutrophil activation because they are repositioned from the nuclear periphery to the more-euchromatic nuclear interior (Denholtz et al., 2020). Therefore, together with ours, all these observations prove that neutrophils are highly plastic cells, able to modify their chromatin after specific stimulations, ultimately promoting the expression of genes that are silent under resting conditions

In addition to LDTFs, sequence motifs for NF-κB and AP-1 (which are proinflammatory SRTFs) emerged from the H3K27Ac ChIP-seq analysis. Although activation of NF-κB by TLR ligands, including R848, has been repeatedly described to occur in human neutrophils (McDonald et al., 1997; Tamassia et al., 2007; Yanagisawa et al., 2009; Zimmermann et al., 2015), that of AP-1 is still under debate (Avdi et al., 2001; Cloutier et al., 2009; Kanai et al., 2004; Tamassia et al., 2007). Studies are currently ongoing in our laboratory to precisely identify the nature of the AP-1 complex inducible in R848-treated neutrophils. In any case, because LDTFs select enhancers in a cell-specific manner, our data suggest that the transcriptional response triggered in neutrophils by TLR8 engagement is regulated by the interplay undergoing between specific myeloid LDTFs families and typical SRTFs (Glass and Natoli, 2016).

An unpredicted finding that emerged from the H3K27Ac ChIP-seq made in R848-activated neutrophils was the enrichment of an octamer motif known to be bound by OCT TFs (namely 5'-ATGCAAAT-3') (Malik et al., 2018; Zhao, 2013). Such an octamer motif was also found in close proximity to the R848-induced PU.1 and C/EBPβ binding sites. Based on gene and protein expression analysis, we could then identify OCT2/POU2F2 as the member of the OCT family binding to the octamer motif in R848-stimulated neutrophils. In fact, kinetics of transcriptional expression revealed that OCT2, although constitutively present at low levels in neutrophils, is markedly upregulated in response to R848, not only at the mRNA, but also at the protein, level. In that context, although OCT2 is preferentially expressed in human B cells (Bargou et al., 1996), murine neuronal cells (Theodorou et al., 2009), and, although at lower levels, murine (Lu et al., 2007) and human

macrophages, monocytes (Neumann et al., 2000) and MONO-MAC (a monocytic cell line) (Bargou et al., 1996), earlier studies reported an upregulation of OCT2 by TLR4 agonists in murine B cells (Corcoran et al., 2004; Kilzheimer et al., 2015) and macrophages (Lu et al., 2007), at both transcriptional and protein level. Moreover, *OCT2* mRNA induction in B lymphocyte precursors was shown to depend on NF-κB activation (Bendall et al., 1997), which is consistent with our previous data on the capacity of R848 to potently activate NF-κB (Zimmermann et al., 2015), as well as with our current observations on the ability of both LPS and TNF-α (other stimuli activating NF-κB in human neutrophils [McDonald et al., 1997]) to induce OCT2 expression and DNA-binding in neutrophils. Because it is known that the concurrent engagement of different TLRs in DCs and macrophages triggers additive/synergistic production of proinflammatory cytokines (Mäkelä et al., 2009), we do not exclude that, also in neutrophils, stimulation via TLR8 in combination with TLR4 agonists may result in an additive or synergistic induction of OCT2 expression and, in turn, OCT2-target genes.

Subsequent genome-wide analysis of OCT2-binding, in resting and R848-activated neutrophils, revealed that OCT2 is constitutively bound to promoter and enhancer regions of hundred genes under resting conditions. However, upon TLR8 engagement, OCT2 is recruited to more than 9,000 *cis*-regulatory elements near immune-related genes, including cytokines (*CXCL8*, *TNF*, *CCL3*/*CCL4*, *IL6*, *IL1A*/*IL1B*, *IL12B*, and *IL23A*), kinases (*IRAK3* and *LYN*), and the co-activator *NFKBIZ*, matching the most-enriched GO terms identified as associated with upregulated genes in TLR8-activated neutrophils. Noteworthy, most of the OCT2-binding sites gained after TLR8 activation were found located in genomic regions associated with enhancer activities, such as intronic and intergenic regions, as well as colocalized with both PU.1 and C/EBPβ cistromes, similar to what observed in B cells for PU.1 (Heinz et al., 2010; Hodson et al., 2016; Solomon et al., 2015), but not C/EBPβ (because it is not expressed in mature B cells) (Pal et al., 2009).

We also performed OCT2 ChIP-seq in resting and R848-treated monocytes. OCT2 protein is known to be constitutively expressed in human monocytes and downregulated during their *in vitro* maturation to dendritic cells but not to macrophages (Neumann et al., 2000). Comparison between neutrophils and autologous monocytes in terms of target binding sites of OCT2-induced peaks revealed that a consistent fraction of them was present in both cell types, whereas others were monocyte or neutrophil specific. Notably, cell-specific peaks were found as associated with genes selectively expressed in the corresponding cell type. In agreement with the notion that a given TF may have discrete binding sites in different cell types, depending on the accessibility of the chromatin, in turn, defined by cell-specific LDTFs (Heinz et al., 2010; Heinz et al., 2015).

OCT2-deficient mice die shortly after birth, indicating an essential role of OCT2 in postnatal survival (Corcoran et al., 1993). Although the functions of OCT2 have been extensively studied in B cells, in which they are associated with B cell maturation, serum immunoglobulin (Ig) levels, and effector responses to *in vitro* stimulation (Zhao, 2013), they are poorly known in myeloid cells. Studies performed in RAW264.7 macrophages have demonstrated that, upon LPS stimulation, OCT2 regulates the expression of inducible nitric oxide synthase (iNOS) and G-CSF (Chou et al., 2011; Lu et al., 2009). Interestingly, G-CSF, but not iNOS, expression is induced also in R848-treated neutrophils, being OCT2 recruited at the G-CSF genomic locus. Moreover, an elegant study made in fetal liver macrophages revealed that OCT2, together with OCT1, binds to an LPS-induced enhancer located 10 kb upstream of the *il12b* TSS. Authors found that the OCT binding site appears important for nucleosome remodeling at this enhancer region, suggesting that OCT proteins are responsible for stimulating the chromatin remodeling events required for full enhancer function (Zhou et al., 2007). This hypothesis is in line with the fact that in human neutrophils, OCT2 is also enriched at the genomic regions that undergo profound epigenetic changes upon TLR8 activation, including *IL12B*. Results obtained in HL-60 cells differentiated into neutrophils, in which OCT2 protein expression was greatly reduced by RNA interference, confirmed its activatory role for many inflammatory genes. However, none of the R848-induced transcripts was abrogated by OCT2 depletion, indicating that this TF is required for amplifying their expression.

We would thus speculate that, in human neutrophils, OCT2 functions similarly to C/EBPδ. The latter TF, like OCT2 in neutrophils, is not expressed in resting murine macrophages but is induced upon LPS stimulation, in turn, sustaining the expression of several inflammatory genes in collaboration with NF-κB (Litvak et al., 2009). Consistently, our findings suggest that OCT2 is directly involved, along with LDTFs and SRTFs, in the delayed control of the transcriptional output triggered in TLR8-activated neutrophils, thereby, functioning as an amplifier of the transcriptional response.

STAR★METHODS

Detailed methods are provided in the online version of this paper and include the following:

- KEY RESOURCES TABLE
- RESOURCE AVAILABILITY
  - Lead contact
  - Materials availability
  - Data and code availability
- EXPERIMENTAL MODEL AND SUBJECT DETAILS
  - Study approval
- METHOD DETAILS
  - Cell purification and culture
  - HL-60 cell differentiation and OCT2 silencing
  - RNA purification
  - qRT-PCR
  - RNA sequencing (RNA-seq) library preparation
  - Immunoblots
  - Chromatin immunoprecipitation (ChIP) assay
  - ChIP sequencing (ChIP-seq)
- QUANTIFICATION AND STATISTICAL ANALYSIS
  - RNA-seq computational analysis
  - ChIP-seq bioinformatic analysis
  - Identification of TF peaks in ChIP-seqs
  - Identification of H3K27Ac-enriched regions by ChIP-seq

- Differential peak analysis
- Scatterplots and heatmaps
- Gene ontology (GO) enrichment analysis
- Gene ontology (GO) of differentially expressed genes
- Integrative analysis of OCT2 ChIP-seq and expression data
- Gene set enrichment analysis (GSEA)
- Statistical analysis

SUPPLEMENTAL INFORMATION

Supplemental information can be found online at https://doi.org/10.1016/j.celrep.2021.109143.

ACKNOWLEDGMENTS

We thank A. Pasqualato (European Institute of Oncology, Milan, Italy) for providing reagents; and especially Monica Castellucci at the Centro Piattaforme Tecnologiche (University of Verona, Verona, Italy) for transcriptome sequencing. This work was supported by grants from Associazione Italiana per la Ricerca sul Cancro (AIRC; IG-20339) and Ministero dell'Istruzione, dell'Università e della Ricerca (PRIN 2015YYKPNN_002 and 20177J4E75_004) to M.A.C.; from Ministero della Salute (GR-2016-02361263) to N.T.; and from the Cariplo Foundation (grant 2015–0584) to G.N. and M.A.C.

AUTHOR CONTRIBUTIONS

N.T., F.B.-A., S.G., S.P., E.G., and R.O. performed all experiments. N.T. and F.B.-A. performed data analysis. R.O. and G.N. contributed to discussions. N.T., G.N., and M.A.C. supervised the project and wrote the manuscript.

DECLARATION OF INTERESTS

The authors declare no competing interests.

Received: October 27, 2020
Revised: March 27, 2021
Accepted: April 26, 2021
Published: May 18, 2021

REFERENCES

Anderson, K.L., Smith, K.A., Pio, F., Torbett, B.E., and Maki, R.A. (1998). Neutrophils deficient in PU.1 do not terminally differentiate or become functionally competent. Blood *92*, 1576–1585.

Arruda-Silva, F., Bianchetto-Aguilera, F., Gasperini, S., Polletti, S., Cosentino, E., Tamassia, N., and Cassatella, M.A. (2017). Human neutrophils produce CCL23 in response to various TLR-agonists and TNFα. Front. Cell. Infect. Microbiol. *7*, 176.

Avdi, N.J., Nick, J.A., Whitlock, B.B., Billstrom, M.A., Henson, P.M., Johnson, G.L., and Worthen, G.S. (2001). Tumor necrosis factor-α activation of the c-Jun N-terminal kinase pathway in human neutrophils. Integrin involvement in a pathway leading from cytoplasmic tyrosine kinases apoptosis. J. Biol. Chem. *276*, 2189–2199.

Bargou, R.C., Leng, C., Krappmann, D., Emmerich, F., Mapara, M.Y., Bommert, K., Royer, H.D., Scheidereit, C., and Dörken, B. (1996). High-level nuclear NF-κB and Oct-2 is a common feature of cultured Hodgkin/Reed-Sternberg cells. Blood *87*, 4340–4347.

Bendall, H.H., Scherer, D.C., Edson, C.R., Ballard, D.W., and Oltz, E.M. (1997). Transcription factor NF-κB regulates inducible Oct-2 gene expression in precursor B lymphocytes. J. Biol. Chem. *272*, 28826–28828.

Bray, N.L., Pimentel, H., Melsted, P., and Pachter, L. (2016). Near-optimal probabilistic RNA-seq quantification. Nat. Biotechnol. *34*, 525–527.

Calzetti, F., Tamassia, N., Arruda-Silva, F., Gasperini, S., and Cassatella, M.A. (2017). The importance of being "pure" neutrophils. J. Allergy Clin. Immunol. *139*, 352–355.e6.

Cassatella, M.A., Gardiman, E., Arruda-Silva, F., Bianchetto-Aguilera, F., Gasperini, S., Bugatti, M., Vermi, W., Larousserie, F., Devergne, O., and Tamassia, N. (2020). Human neutrophils activated by TLR8 agonists, with or without IFN-gamma, synthesize and release EBI3, but not IL-12, IL-27, IL-35, or IL-39. J. Leukoc. Biol. *108*, 1515–1526.

Chi, H., Li, C., Zhao, F.S., Zhang, L., Ng, T.B., Jin, G., and Sha, O. (2017). Anti-tumor activity of toll-like receptor 7 agonists. Front. Pharmacol. *8*, 304.

Chou, Y.Y., Gao, J.I., Chang, S.F., Chang, P.Y., and Lu, S.C. (2011). Rapamycin inhibits lipopolysaccharide induction of granulocyte-colony stimulating factor and inducible nitric oxide synthase expression in macrophages by reducing the levels of octamer-binding factor-2. FEBS J. *278*, 85–96.

Cloutier, A., Guindi, C., Larivée, P., Dubois, C.M., Amrani, A., and McDonald, P.P. (2009). Inflammatory cytokine production by human neutrophils involves C/EBP transcription factors. J. Immunol. *182*, 563–571.

Collins, S.J., Ruscetti, F.W., Gallagher, R.E., and Gallo, R.C. (1978). Terminal differentiation of human promyelocytic leukemia cells induced by dimethyl sulfoxide and other polar compounds. Proc. Natl. Acad. Sci. USA *75*, 2458–2462.

Corcoran, L.M., Karvelas, M., Nossal, G.J., Ye, Z.S., Jacks, T., and Baltimore, D. (1993). Oct-2, although not required for early B-cell development, is critical for later B-cell maturation and for postnatal survival. Genes Dev. *7*, 570–582.

Corcoran, L.M., Koentgen, F., Dietrich, W., Veale, M., and Humbert, P.O. (2004). All known *in vivo* functions of the Oct-2 transcription factor require the C-terminal protein domain. J. Immunol. *172*, 2962–2969.

Cotney, J., Leng, J., Oh, S., DeMare, L.E., Reilly, S.K., Gerstein, M.B., and Noonan, J.P. (2012). Chromatin state signatures associated with tissue-specific gene expression and enhancer activity in the embryonic limb. Genome Res. *22*, 1069–1080.

Denholtz, M., Zhu, Y., He, Z., Lu, H., Isoda, T., Döhrmann, S., Nizet, V., and Murre, C. (2020). Upon microbial challenge, human neutrophils undergo rapid changes in nuclear architecture and chromatin folding to orchestrate an immediate inflammatory gene program. Genes Dev. *34*, 149–165.

Ear, T., and McDonald, P.P. (2008). Cytokine generation, promoter activation, and oxidant-independent NF-kappaB activation in a transfectable human neutrophilic cellular model. BMC Immunol. *9*, 14.

ENCODE Project Consortium (2011). A user's guide to the encyclopedia of DNA elements (ENCODE). PLoS Biol. *9*, e1001046.

Fischer, J., Walter, C., Tönges, A., Aleth, H., Jordão, M.J.C., Leddin, M., Gröning, V., Erdmann, T., Lenz, G., Roth, J., et al. (2019). Safeguard function of PU.1 shapes the inflammatory epigenome of neutrophils. Nat. Immunol. *20*, 546–558.

Gaudreault, E., and Gosselin, J. (2009). Leukotriene B4 potentiates CpG signaling for enhanced cytokine secretion by human leukocytes. J. Immunol. *183*, 2650–2658.

Ghisletti, S., Barozzi, I., Mietton, F., Polletti, S., De Santa, F., Venturini, E., Gregory, L., Lonie, L., Chew, A., Wei, C.L., et al. (2010). Identification and characterization of enhancers controlling the inflammatory gene expression program in macrophages. Immunity *32*, 317–328.

Glass, C.K., and Natoli, G. (2016). Molecular control of activation and priming in macrophages. Nat. Immunol. *17*, 26–33.

Guilliams, M., Mildner, A., and Yona, S. (2018). Developmental and functional heterogeneity of monocytes. Immunity *49*, 595–613.

Häger, M., Cowland, J.B., and Borregaard, N. (2010). Neutrophil granules in health and disease. J. Intern. Med. *268*, 25–34.

Hayashi, F., Means, T.K., and Luster, A.D. (2003). Toll-like receptors stimulate human neutrophil function. Blood *102*, 2660–2669.

Heinz, S., Benner, C., Spann, N., Bertolino, E., Lin, Y.C., Laslo, P., Cheng, J.X., Murre, C., Singh, H., and Glass, C.K. (2010). Simple combinations of lineage-determining transcription factors prime *cis*-regulatory elements required for macrophage and B cell identities. Mol. Cell *38*, 576–589.

Heinz, S., Romanoski, C.E., Benner, C., Allison, K.A., Kaikkonen, M.U., Orozco, L.D., and Glass, C.K. (2013). Effect of natural genetic variation on enhancer selection and function. Nature *503*, 487–492.

Heinz, S., Romanoski, C.E., Benner, C., and Glass, C.K. (2015). The selection and function of cell type-specific enhancers. Nat. Rev. Mol. Cell Biol. *16*, 144–154.

Hodson, D.J., Shaffer, A.L., Xiao, W., Wright, G.W., Schmitz, R., Phelan, J.D., Yang, Y., Webster, D.E., Rui, L., Kohlhammer, H., et al. (2016). Regulation of normal B-cell differentiation and malignant B-cell survival by OCT2. Proc. Natl. Acad. Sci. USA *113*, E2039–E2046.

Jakubzick, C.V., Randolph, G.J., and Henson, P.M. (2017). Monocyte differentiation and antigen-presenting functions. Nat. Rev. Immunol. *17*, 349–362.

Jalili, V., Matteucci, M., Masseroli, M., and Morelli, M.J. (2015). Using combined evidence from replicates to evaluate ChIP-seq peaks. Bioinformatics *31*, 2761–2769.

Kaikkonen, M.U., Spann, N.J., Heinz, S., Romanoski, C.E., Allison, K.A., Stender, J.D., Chun, H.B., Tough, D.F., Prinjha, R.K., Benner, C., and Glass, C.K. (2013). Remodeling of the enhancer landscape during macrophage activation is coupled to enhancer transcription. Mol. Cell *51*, 310–325.

Kanai, K., Asano, K., Hisamitsu, T., and Suzaki, H. (2004). Suppression of matrix metalloproteinase-9 production from neutrophils by a macrolide antibiotic, roxithromycin, *in vitro*. Mediators Inflamm. *13*, 313–319.

Kilzheimer, M., Quandt, J., Langhans, J., Weihrich, P., Wirth, T., and Brunner, C. (2015). NF-κB-dependent signals control BOB.1/OBF.1 and Oct2 transcriptional activity in B cells. Eur. J. Immunol. *45*, 3441–3453.

Kundaje, A., Meuleman, W., Ernst, J., Bilenky, M., Yen, A., Heravi-Moussavi, A., Kheradpour, P., Zhang, Z., Wang, J., Ziller, M.J., et al.; Roadmap Epigenomics Consortium (2015). Integrative analysis of 111 reference human epigenomes. Nature *518*, 317–330.

Langmead, B., Trapnell, C., Pop, M., and Salzberg, S.L. (2009). Ultrafast and memory-efficient alignment of short DNA sequences to the human genome. Genome Biol. *10*, R25.

Lester, S.N., and Li, K. (2014). Toll-like receptors in antiviral innate immunity. J. Mol. Biol. *426*, 1246–1264.

Ley, K., Hoffman, H.M., Kubes, P., Cassatella, M.A., Zychlinsky, A., Hedrick, C.C., and Catz, S.D. (2018). Neutrophils: new insights and open questions. Sci. Immunol. *3*, eaat4579.

Li, H., Liu, L., Zhang, D., Xu, J., Dai, H., Tang, N., Su, X., and Cao, B. (2020). SARS-CoV-2 and viral sepsis: observations and hypotheses. Lancet *395*, 1517–1520.

Litvak, V., Ramsey, S.A., Rust, A.G., Zak, D.E., Kennedy, K.A., Lampano, A.E., Nykter, M., Shmulevich, I., and Aderem, A. (2009). Function of C/EBPδ in a regulatory circuit that discriminates between transient and persistent TLR4-induced signals. Nat. Immunol. *10*, 437–443.

Love, M.I., Huber, W., and Anders, S. (2014). Moderated estimation of fold change and dispersion for RNA-seq data with DESeq2. Genome Biol. *15*, 550.

Lu, S.C., Chang, S.F., Chen, H.L., Chou, Y.Y., Lan, Y.H., Chuang, C.Y., Yu, W.H., and Chen, C.L. (2007). A novel role for Oct-2 in the lipopolysaccharide-mediated induction of resistin gene expression in RAW264.7 cells. Biochem. J. *402*, 387–395.

Lu, S.C., Wu, H.W., Lin, Y.J., and Chang, S.F. (2009). The essential role of Oct-2 in LPS-induced expression of iNOS in RAW 264.7 macrophages and its regulation by trichostatin A. Am. J. Physiol. Cell Physiol. *296*, C1133–C1139.

Lu, H., Dietsch, G.N., Matthews, M.A., Yang, Y., Ghanekar, S., Inokuma, M., Suni, M., Maino, V.C., Henderson, K.E., Howbert, J.J., et al. (2012). VTX-2337 is a novel TLR8 agonist that activates NK cells and augments ADCC. Clin. Cancer Res. *18*, 499–509.

Mäkelä, S.M., Strengell, M., Pietilä, T.E., Osterlund, P., and Julkunen, I. (2009). Multiple signaling pathways contribute to synergistic TLR ligand-dependent cytokine gene expression in human monocyte-derived macrophages and dendritic cells. J. Leukoc. Biol. *85*, 664–672.

Malik, V., Zimmer, D., and Jauch, R. (2018). Diversity among POU transcription factors in chromatin recognition and cell fate reprogramming. Cell. Mol. Life Sci. *75*, 1587–1612.

McDonald, P.P., Bald, A., and Cassatella, M.A. (1997). Activation of the NF-κB pathway by inflammatory stimuli in human neutrophils. Blood *89*, 3421–3433.

McLean, C.Y., Bristor, D., Hiller, M., Clarke, S.L., Schaar, B.T., Lowe, C.B., Wenger, A.M., and Bejerano, G. (2010). GREAT improves functional interpretation of *cis*-regulatory regions. Nat. Biotechnol. *28*, 495–501.

Mildner, A., Schönheit, J., Giladi, A., David, E., Lara-Astiaso, D., Lorenzo-Vivas, E., Paul, F., Chappell-Maor, L., Priller, J., Leutz, A., et al. (2017). Genomic characterization of murine monocytes reveals C/EBPβ transcription factor dependence of Ly6C$^-$ cells. Immunity *46*, 849–862.e7.

Moreno-Eutimio, M.A., López-Macías, C., and Pastelin-Palacios, R. (2020). Bioinformatic analysis and identification of single-stranded RNA sequences recognized by TLR7/8 in the SARS-CoV-2, SARS-CoV, and MERS-CoV genomes. Microbes Infect. *22*, 226–229.

Morse, S.M., Shaw, G., and Larner, S.F. (2006). Concurrent mRNA and protein extraction from the same experimental sample using a commercially available column-based RNA preparation kit. Biotechniques *40*, 54, 56, 58.

Muller, P.Y., Janovjak, H., Miserez, A.R., and Dobbie, Z. (2002). Processing of gene expression data generated by quantitative real-time RT-PCR. Biotechniques *32*, 1372–1374, 1376, 1378–1379.

Nagase, H., Okugawa, S., Ota, Y., Yamaguchi, M., Tomizawa, H., Matsushima, K., Ohta, K., Yamamoto, K., and Hirai, K. (2003). Expression and function of Toll-like receptors in eosinophils: activation by Toll-like receptor 7 ligand. J. Immunol. *171*, 3977–3982.

Nathan, C. (2020). Neutrophils and COVID-19: Nots, NETs, and knots. J. Exp. Med. *217*, e20201439.

Neumann, M., Fries, H., Scheicher, C., Keikavoussi, P., Kolb-Mäurer, A., Bröcker, E., Serfling, E., and Kämpgen, E. (2000). Differential expression of Rel/NF-κB and octamer factors is a hallmark of the generation and maturation of dendritic cells. Blood *95*, 277–285.

Novakovic, B., Habibi, E., Wang, S.Y., Arts, R.J.W., Davar, R., Megchelenbrink, W., Kim, B., Kuznetsova, T., Kox, M., Zwaag, J., et al. (2016). β-glucan reverses the epigenetic state of LPS-induced immunological tolerance. Cell *167*, 1354–1368.e14.

Ostuni, R., and Natoli, G. (2013). Lineages, cell types and functional states: a genomic view. Curr. Opin. Cell Biol. *25*, 759–764.

Ostuni, R., Piccolo, V., Barozzi, I., Polletti, S., Termanini, A., Bonifacio, S., Curina, A., Prosperini, E., Ghisletti, S., and Natoli, G. (2013). Latent enhancers activated by stimulation in differentiated cells. Cell *152*, 157–171.

Ostuni, R., Natoli, G., Cassatella, M.A., and Tamassia, N. (2016). Epigenetic regulation of neutrophil development and function. Semin. Immunol. *28*, 83–93.

Pal, R., Janz, M., Galson, D.L., Gries, M., Li, S., Jöhrens, K., Anagnostopoulos, I., Dörken, B., Mapara, M.Y., Borghesi, L., et al. (2009). C/EBPbeta regulates transcription factors critical for proliferation and survival of multiple myeloma cells. Blood *114*, 3890–3898.

Patro, R., Duggal, G., Love, M.I., Irizarry, R.A., and Kingsford, C. (2017). Salmon provides fast and bias-aware quantification of transcript expression. Nat. Methods *14*, 417–419.

Pham, T.H., Benner, C., Lichtinger, M., Schwarzfischer, L., Hu, Y., Andreesen, R., Chen, W., and Rehli, M. (2012). Dynamic epigenetic enhancer signatures reveal key transcription factors associated with monocytic differentiation states. Blood *119*, e161–e171.

Picelli, S., Faridani, O.R., Björklund, A.K., Winberg, G., Sagasser, S., and Sandberg, R. (2014). Full-length RNA-seq from single cells using Smart-seq2. Nat. Protoc. *9*, 171–181.

Ramírez, F., Ryan, D.P., Grüning, B., Bhardwaj, V., Kilpert, F., Richter, A.S., Heyne, S., Dündar, F., and Manke, T. (2016). deepTools2: a next generation web server for deep-sequencing data analysis. Nucleic Acids Res. *44* (*W1*), W160–W165.

Ross-Innes, C.S., Stark, R., Teschendorff, A.E., Holmes, K.A., Ali, H.R., Dunning, M.J., Brown, G.D., Gojis, O., Ellis, I.O., Green, A.R., et al. (2012). Differential oestrogen receptor binding is associated with clinical outcome in breast cancer. Nature *481*, 389–393.

Scapini, P., and Cassatella, M.A. (2014). Social networking of human neutrophils within the immune system. Blood *124*, 710–719.

Solomon, L.A., Li, S.K., Piskorz, J., Xu, L.S., and DeKoter, R.P. (2015). Genome-wide comparison of PU.1 and Spi-B binding sites in a mouse B lymphoma cell line. BMC Genomics *16*, 76.

Subramanian, A., Tamayo, P., Mootha, V.K., Mukherjee, S., Ebert, B.L., Gillette, M.A., Paulovich, A., Pomeroy, S.L., Golub, T.R., Lander, E.S., and Mesirov, J.P. (2005). Gene set enrichment analysis: a knowledge-based approach for interpreting genome-wide expression profiles. Proc. Natl. Acad. Sci. USA *102*, 15545–15550.

Tamassia, N., and Cassatella, M.A. (2013). Cytoplasmic receptors recognizing nucleic acids and mediating immune functions in neutrophils. Curr. Opin. Pharmacol. *13*, 547–554.

Tamassia, N., Le Moigne, V., Calzetti, F., Donini, M., Gasperini, S., Ear, T., Cloutier, A., Martinez, F.O., Fabbri, M., Locati, M., et al. (2007). The MyD88-independent pathway is not mobilized in human neutrophils stimulated via TLR4. J. Immunol. *178*, 7344–7356.

Tamassia, N., Castellucci, M., Rossato, M., Gasperini, S., Bosisio, D., Giacomelli, M., Badolato, R., Cassatella, M.A., and Bazzoni, F. (2010). Uncovering an IL-10-dependent NF-κB recruitment to the IL-1ra promoter that is impaired in STAT3 functionally defective patients. FASEB J. *24*, 1365–1375.

Tamassia, N., Zimmermann, M., Castellucci, M., Ostuni, R., Bruderek, K., Schilling, B., Brandau, S., Bazzoni, F., Natoli, G., and Cassatella, M.A. (2013). Cutting edge: an inactive chromatin configuration at the IL-10 locus in human neutrophils. J. Immunol. *190*, 1921–1925.

Tamassia, N., Bianchetto-Aguilera, F., Arruda-Silva, F., Gardiman, E., Gasperini, S., Calzetti, F., and Cassatella, M.A. (2018). Cytokine production by human neutrophils: revisiting the "dark side of the moon". Eur. J. Clin. Invest. *48* (*Suppl 2*), e12952.

Tamassia, N., Arruda-Silva, F., Wright, H.L., Moots, R.J., Gardiman, E., Bianchetto-Aguilera, F., Gasperini, S., Capone, M., Maggi, L., Annunziato, F., et al. (2019). Human neutrophils activated via TLR8 promote Th17 polarization through IL-23. J. Leukoc. Biol. *105*, 1155–1165.

Temizoz, B., Kuroda, E., and Ishii, K.J. (2018). Combination and inducible adjuvants targeting nucleic acid sensors. Curr. Opin. Pharmacol. *41*, 104–113.

Theodorou, E., Dalembert, G., Heffelfinger, C., White, E., Weissman, S., Corcoran, L., and Snyder, M. (2009). A high throughput embryonic stem cell screen identifies Oct-2 as a bifunctional regulator of neuronal differentiation. Genes Dev. *23*, 575–588.

Thomas, C.J., and Schroder, K. (2013). Pattern recognition receptor function in neutrophils. Trends Immunol. *34*, 317–328.

Tibshirani, R., Walther, G., and Hastie, T. (2001). Estimating the number of clusters in a data set via the gap statistic. J. R. Stat. Soc. Series B Stat. Methodol. *63*, 411–423.

Ugolini, M., Gerhard, J., Burkert, S., Jensen, K.J., Georg, P., Ebner, F., Volkers, S.M., Thada, S., Dietert, K., Bauer, L., et al. (2018). Recognition of microbial viability via TLR8 drives T_{FH} cell differentiation and vaccine responses. Nat. Immunol. *19*, 386–396.

Vierbuchen, T., Stein, K., and Heine, H. (2019). RNA is taking its toll: impact of RNA-specific Toll-like receptors on health and disease. Allergy *74*, 223–235.

Wang, S., Sun, H., Ma, J., Zang, C., Wang, C., Wang, J., Tang, Q., Meyer, C.A., Zhang, Y., and Liu, X.S. (2013). Target analysis by integration of transcriptome and ChIP-seq data with BETA. Nat. Protoc. *8*, 2502–2515.

Yamamoto, M., Yamazaki, S., Uematsu, S., Sato, S., Hemmi, H., Hoshino, K., Kaisho, T., Kuwata, H., Takeuchi, O., Takeshige, K., et al. (2004). Regulation of Toll/IL-1-receptor-mediated gene expression by the inducible nuclear protein IκBζ. Nature *430*, 218–222.

Yanagisawa, S., Koarai, A., Sugiura, H., Ichikawa, T., Kanda, M., Tanaka, R., Akamatsu, K., Hirano, T., Matsunaga, K., Minakata, Y., and Ichinose, M. (2009). Oxidative stress augments toll-like receptor 8 mediated neutrophilic responses in healthy subjects. Respir. Res. *10*, 50.

Yu, G., Wang, L.G., Han, Y., and He, Q.Y. (2012). clusterProfiler: an R package for comparing biological themes among gene clusters. OMICS *16*, 284–287.

Zhang, S., Hu, Z., Tanji, H., Jiang, S., Das, N., Li, J., Sakaniwa, K., Jin, J., Bian, Y., Ohto, U., et al. (2018). Small-molecule inhibition of TLR8 through stabilization of its resting state. Nat. Chem. Biol. *14*, 58–64.

Zhao, F.Q. (2013). Octamer-binding transcription factors: genomics and functions. Front. Biosci. *18*, 1051–1071.

Zhou, L., Nazarian, A.A., Xu, J., Tantin, D., Corcoran, L.M., and Smale, S.T. (2007). An inducible enhancer required for Il12b promoter activity in an insulated chromatin environment. Mol. Cell. Biol. *27*, 2698–2712.

Zimmermann, M., Aguilera, F.B., Castellucci, M., Rossato, M., Costa, S., Lunardi, C., Ostuni, R., Girolomoni, G., Natoli, G., Bazzoni, F., et al. (2015). Chromatin remodelling and autocrine TNFα are required for optimal interleukin-6 expression in activated human neutrophils. Nat. Commun. *6*, 6061.

Zimmermann, M., Arruda-Silva, F., Bianchetto-Aguilera, F., Finotti, G., Calzetti, F., Scapini, P., Lunardi, C., Cassatella, M.A., and Tamassia, N. (2016). IFNα enhances the production of IL-6 by human neutrophils activated via TLR8. Sci. Rep. *6*, 19674.

STAR★METHODS

KEY RESOURCES TABLE

REAGENT or RESOURCE	SOURCE	IDENTIFIER
Antibodies		
Rabbit polyclonal anti-OCT2	Santa Cruz Biotechnology	Cat# sc-233; RRID: AB_2167205
Rabbit polyclonal anti-PU.1	Santa Cruz Biotechnology	Cat# sc-352; RRID: AB_632289
Rabbit polyclonal anti-OCT1	Santa Cruz Biotechnology	Cat# sc-232; RRID: AB_2167065
Rabbit polyclonal anti-C/EBPβ	Santa Cruz Biotechnology	Cat# sc-151; RRID: AB_2260363
Rabbit polyclonal anti-OCT2	Abcam	Cat# ab179808; RRID: AB_2889931
Rabbit polyclonal anti-H3K27Ac	Abcam	Cat# ab4729; RRID: AB_2118291
Rabbit polyclonal anti-actin	Sigma-Aldrich	Cat# A5060; RRID:AB_476738
Mouse monoclonal anti-tubulin	Sigma-Aldrich	Cat# T5293; RRID: AB_477580
Rabbit polyclonal anti-histone H3	Santa Cruz Biotechnology	Cat# sc-10809; RRID: AB_2115276
Biological samples		
Buffy coats from human blood	Transfusion Center, university hospital, Verona,	N/A
Chemicals, peptides, and recombinant proteins		
Fast SYBR Green Master Mix	ThermoFisher	Cat# 4385612
R848	Invivogen	Cat# tlrl-r848
LPS	Invivogen	Cat# tlrl-3pelps
VTX-2337	Selleck Chem	Cat# S7161
TNFα	R&D Systems	Cat# 210-TA
G-CSF	Italfarmaco Spa	Cat# Myelostim
Dynabeads Protein A for Immunoprecipitation	ThermoFisher	Cat# 10001D
Critical commercial assays		
RNeasy Mini Kit	QIAGEN	Cat# 74104
QIAquick PCR Purification Kit	QIAGEN	Cat# 28104
Ingenio Electroporation Solution	Myrus	Cat# MIR 50115
EasySep neutrophil enrichment kit	StemCell Technology	Cat# 19257
CD14 MicroBeads, human	Miltenyi Biotec	Cat# 130-050-201
Qubit dsDNA HS Assay Kit	ThermoFisher	Cat# Q32854
High Sensitivity D5000 ScreenTape	Agilent	Cat# 5067-5592
TruSeq ChIP Library Preparation Kit	Illumina	Cat# IP-202-1012
NextSeq 500/550 High Output v2.5 kit (75 cycles)	Illumina	Cat# 20024906
Deposited data		
RNA-seq and ChIP-seq	This paper	GEO: GSE119395
Experimental models: Cell lines		
Human: HL-60 cells	ATCC	Cat# CCL-240
Human: RAJI cells	DMSZ	Cat# ACC 319
Human: DAUDI cells	DMSZ	Cat# ACC 78
Oligonucleotides		
ON-TARGETplus OCT2 siRNA	Dharmacon	Cat# L-019690-00-0005
ON-TARGETplus Non-targeting Pool	Dharmacon	Cat# D-001810-10-05
ISPCR	(Picelli et al., 2014) ThermoFisher	N/A
Oligo-dT	(Picelli et al., 2014) ThermoFisher	N/A

(*Continued on next page*)

Continued

REAGENT or RESOURCE	SOURCE	IDENTIFIER
Template Switch Oligo (TSO)	(Picelli et al., 2014) Exiqon	N/A
Primers for mRNA expression, see Table S7	This paper	N/A
Primers for ChIP-qPCR, see Table S8	This paper	N/A
Software and algorithms		
GraphPad Prism 7	GraphPad Software, Inc	https://www.graphpad.com:443/scientific-software/prism/
Salmon v0.9.1	Patro et al., 2017	https://combine-lab.github.io/salmon/
DESeq2 version 1.20.0	Love et al., 2014	https://bioconductor.org/packages/release/bioc/html/DESeq2.html
Tximport version 1.80	Patro et al., 2017	https://bioconductor.org/packages/release/bioc/html/tximport.html
clusterProfile version	Yu et al., 2012	https://bioconductor.org/packages/release/bioc/html/clusterProfiler.html
Bowtie version 1.0.0	Langmead et al., 2009	http://bowtie-bio.sourceforge.net/index.shtml
HOMER version 4.7.2	Heinz et al., 2010	http://homer.ucsd.edu/homer/
GREAT version 3.0.0	McLean et al., 2010	http://bejerano.stanford.edu/great/public/html/
BETA version 1.0.7	Wang et al., 2013	http://cistrome.org/BETA/

RESOURCE AVAILABILITY

Lead contact

Further information and requests for resources and reagents should be directed to and will be fulfilled by the lead contact, Marco A. Cassatella (marco.cassatella@univr.it).

Materials availability

This study did not generate new unique reagents.

Data and code availability

The RNA-seq and ChIP-seq datasets generated in this study are available at the Gene Expression Omnibus database (https://www.ncbi.nlm.nih.gov/geo/) under the accession number GEO: GSE119395.

EXPERIMENTAL MODEL AND SUBJECT DETAILS

Study approval

Buffy coats were obtained from the Blood Center of Verona hospital, following informed written consent by anonymous healthy donors. Gender and age of healthy donors were not provided. The study has been cleared by the Ethics Committee of the Azienda Ospedaliera Universitaria Integrata di Verona (Italy).

METHOD DETAILS

Cell purification and culture

Granulocytes were isolated from buffy coats of healthy donors and manipulated under endotoxin-free conditions. After Ficoll-Paque gradient centrifugation, followed by dextran sedimentation and hypotonic lysis of erythrocytes, neutrophils were isolated to reach 99.7 ± 0.2% purity, by positively removing any eventual contaminating cells using the EasySep neutrophil enrichment kit (StemCell Technology, Vancouver, Canada) (Calzetti et al., 2017). Human $CD14^+$-monocytes were isolated from PBMCs by anti-CD14 microbeads (Miltenyi Biotec, Bergisch Gladbach, Germany) to reach > 98% purity. Neutrophils and monocytes were then suspended at $5x10^6$/ml and $3x10^6$/ml, respectively, in RPMI 1640 medium supplemented with 10% low endotoxin FBS (< 0.5 EU/ml; from Sigma, Saint Louis, MO, USA), treated or not with 5 μM R848 (InvivoGen, San Diego, CA, USA), 1 μM VTX-2337 (Selleck Chem, Boston, MA, USA), 1 μg/ml LPS (ultrapure, *Escherichia coli* 0111:B4 strain, InvivoGen), 10 ng/ml TNFα (R&D Systems, Minneapolis,MN, USA) and 1000 U/ml G-CSF (Myelostim, Italfarmaco Spa, Milano, Italy), seated either in 6/24-well tissue culture plates or polystyrene flasks (Greiner Bio-One, Kremsmüster, Austria) and cultured at 37°, 5% CO_2 atmosphere. After the desired incubation period, cells were

either processed for ChIP-experiments or collected and spun for 5 min at 300x*g* for other assays. Cell pellets were either extracted for total RNA or lysed for protein analysis.

HL-60 cell differentiation and OCT2 silencing

HL-60 cells were cultured at 37°C, 5% CO_2 atmosphere, in RPMI 1640 containing 10% FCS. To induce granulocytic differentiation, HL-60 cells were cultured in 1.25% DMSO-containing culture medium for 5 days, as previously described (Tamassia et al., 2007). Transfection of siRNA was performed by electroporation using Ingenio Electroporation Solution (Myrus), and the Amaxa Nucleofector II device (Lonza). Briefly, at the fourth day of culture in DMSO, 10^7 HL-60 cells were suspended in 100 μL of Ingenio solution containing either 150 pmol of ONTARGET plus Human POU2F2 siRNA pool, or ON-TARGET plus nontargeting siRNA pool (GE Healthcare Dharmacon, Lafayette, CO, USA), and then transferred to a nucleoporation cuvette. Electroporation was performed using the T019 program of the Nucleofector II device. Transfected cells were plated in RPMI 1640 containing 10% FCS for 24 h and, after medium replacement, were incubated with or without 5 μM R848 for further 6 h.

RNA purification

Total RNA was extracted after cell lysis by the RNeasy Mini Kit (QIAGEN, Venlo, Limburg, Netherlands) (Tamassia et al., 2007). To completely remove any possible contaminating DNA, an on-column DNase digestion with the RNase-free DNase set (QIAGEN) was performed during total RNA isolation (Arruda-Silva et al., 2017). Quality control of the total RNA was performed using Agilent TapeStation 2200 (Agilent Technologies). RNA integrity (RIN) was routinely found to be optimal (RIN $\geq$ 7.0).

qRT-PCR

Purified RNA was reverse-transcribed into cDNA using Superscript III (Life Technologies, Carlsbad, CA, USA) and random hexamer primers (Life Technologies), while qPCR was carried out using Fast SYBR® Green Master Mix (Life Technologies) (Arruda-Silva et al., 2017). Sequences of gene-specific primer pairs (Life Technologies) are listed in Table S7. Data were calculated by Q-Gene software (https://www.gene-quantification.de/download.html) and expressed as mean normalized expression (MNE) units after GAPDH or RPL32 normalization (Muller et al., 2002).

RNA sequencing (RNA-seq) library preparation

Libraries for transcriptome analysis were prepared using the Smart-seq2 protocol (Picelli et al., 2014), which permits to obtain a library from less than 500 pg of total RNA. Briefly, 2 ng of total RNA were copied into first strand cDNA by reverse transcription and template-switching oligo (dT) primers and an LNA-containing template-switching oligo (TSO). The resulting cDNA was pre-amplified, purified, and tagmented with Tn5 transposase (kindly gifted by Dr. Sebastiano Pasqualato, European Institute of Oncology, Milan, 20139, Italy). cDNA fragments generated after tagmentation were gap-repaired, enriched by PCR and purified to create the final cDNA library. Libraries were sequenced on the Illumina NextSeq 500 at the Centro Piattaforme Tecnologiche (CPT) of the University of Verona. RNA-seq experiments in neutrophils/monocytes and HL-60 cells were independently performed three and four times, respectively.

Immunoblots

Whole-cell extracts were recovered from the protein-rich flow-through solutions obtained after the first centrifugation step for the RNeasy mini kit (QIAGEN) used for total RNA extraction procedure (Zimmermann et al., 2015). After overnight incubation at −20°C, protein precipitates from the flow-through solutions were washed with pre-chilled 100% ethanol and solubilized in Laemmli sample buffer (Morse et al., 2006). To prepare nuclear and cytoplasmic extracts, $5x10^7$ neutrophils/condition were diluted in ice-cold PBS and centrifuged twice at 300x*g* for 5 min at 4°C. Cells were then suspended in relaxation buffer containing anti-phosphatase and anti-protease cocktails, to be disrupted by nitrogen cavitation (Parr Instruments, Mobile, IL) as described (McDonald et al., 1997). Nuclear, cytoplasmic, and whole-cell extracts were processed for immunoblots by standard procedures (Zimmermann et al., 2015). Nitrocellulose membranes were first blocked in PBS containing 5% BSA for 1 h at room T and then incubated overnight at 4°C in the presence of specific primary antibodies diluted in PBS containing 1% BSA. Blotted proteins were detected and quantified by the Odyssey infrared imaging system (LI-COR Biosciences, Lincoln, NE, USA) (Zimmermann et al., 2015). Rabbit anti-OCT2 pAb (ab179808) were from Abcam (Cambridge, MA, USA), anti-Histone H3 (sc-10809) pAb were purchased from Santa Cruz Biotech (Santa Cruz, CA, USA), while rabbit anti-actin (A5060) pAb and mouse anti-tubulin (T5293) mAb were purchased from Sigma.

Chromatin immunoprecipitation (ChIP) assay

Protein-DNA cross-linking was achieved by incubating $2.5x10^6$ (for histone modification ChIP), or 10^7 (for TF ChIP), neutrophils or monocytes with 1% formaldehyde for 10 min at room T, under gentle agitation. Cross-linking reaction was stopped by adding glycine to a final concentration of 125 mM, and incubating cells at room T for five more minutes. After fixation, cells were washed with ice-cold PBS, collected by scraping, and finally pelleted by centrifugation (5 min, 300x*g*, 4°C). Pellets were suspended in 900 μL L1 lysis buffer (50 mM Tris, pH 8.0, 2 mM EDTA, 0.1% IGEPAL, 10% glycerol) containing protease inhibitors. Nuclei were pelleted at 1000x*g* at 4°C and resuspended in 300 μL L2 lysis buffer (50 mM Tris, pH 8.0, 1% SDS, 5 mM EDTA) including protease inhibitors. Chromatin was sheared to an average DNA size of 300-400 bp by sonication on wet ice [6 pulses of 15 s at the 50% maximum potency, with 15 s

pauses, using a BANDELIN SONOPLUS ultrasonic homogenizers HD 2070 (Bandelin, Berlin, Germany)]. Lysates were then cleared by centrifugation to remove debris (10 min, 13000x*g*, 12°C), and diluted 10x in dilution buffer (50 mM Tris, 5 mM EDTA, 200 mM, 0.5% IGEPAL). Immunoprecipitations were carried out overnight at 4°C using 5 μg/ml antibodies. Immune complexes were then collected by adding 15 μl of Dynabeads Protein A (Thermo Fisher Scientific, Waltham, MA, USA) for 1 h at 4°C under gentle rotation. Beads were then immobilized on a magnetic support and, after keeping 5% of the supernatant (specified in the text as "input" DNA, i.e., unbound DNA used to normalize the amount of immunoprecipitated DNA), washed three times in washing buffer (20 mM Tris, pH 8.0, 0.1% SDS, 2 mM EDTA, 1% IGEPAL, 500 mM NaCl) and once in TE. The resulting protein complexes were then eluted in TE containing 2% SDS, and reversed crosslinked by overnight incubation at 65°C. Antibodies toward PU.1 (sc-352), C/EBPβ (sc-150), OCT1 (sc-232), and OCT2 (sc-233) were purchased from Santa Cruz Biotech, while antibodies toward H3K27Ac (ab4729) and OCT2 (ab179808) were from Abcam. The DNA was purified by QiaQuick PCR purification kit (QIAGEN) according to the manufacturer's instructions and eluted in 50-100 μl. 3 μl of the immunoprecipitated DNA were then used for each quantitative PCR (qPCR) reaction. To establish the background levels of ChIP experiments, the precipitation signal was quantified also at the promoter of prolactin (*PRL*), since it is completely silent in myeloid cells (Tamassia et al., 2010). The coimmunoprecipitated material was subjected to qPCR analysis using specific primers (purchased from Life Technologies) listed in Table S8.

ChIP sequencing (ChIP-seq)

ChIP DNA was prepared for sequencing following TruSeq DNA sample preparation guide (Illumina, Cambridge, UK). In brief, 10-50 ng purified DNA from chromatin immunoprecipitation, obtained from different amounts of cells according to the antibody used for the ChIP, were adaptor-ligated and PCR-amplified according to the manufacturer's protocol (Illumina). Sequencing libraries were multiplexed and ran on Illumina sequencer. Finally, reads were quality-filtered according to the Illumina pipeline (Ostuni and Natoli, 2013). All ChIP-seq experiments were independently repeated two times.

QUANTIFICATION AND STATISTICAL ANALYSIS

RNA-seq computational analysis

Computational analysis of transcriptome datasets generated by Smart-seq2 has been performed using the following bioinformatic pipeline. Raw sequencing output BCL data were converted to FASTQ files by using bcl2fastq v2.20 software. After quality filtering, according to the Illumina pipeline, the contaminant adapters in the FastQ files (single-end 75 bp) were detected using FastQC v0.11.8. Then, adapters and base quality trimming were performed using Trim Galore! (https://www.bioinformatics.babraham.ac.uk/projects/trim_galore/) script with parameters -length 50. To improve the quality of the mapping, reads were further trimmed at the 3′ to a length lower than 72 bp being discarded. Trimmed reads were quantified using Kallisto quant (Bray et al., 2016) to the human reference transcriptome GRCh38v96 obtained from ENSEMBL web site (www.ensembl.org/index.html) and applying parameters –bias –single -l 200 -s 20 –genomebam. Kallisto performs transcript level quantification estimated from Smart-seq2; transcripts were combined to gene level using tximport packages. Gene counts were normalized among various samples using DESeq2, and only genes coding to protein and long non-coding RNA (lnRNA) were retained for downstream analysis. DESeq2 was used to generate the expression metric and fragment per kilobase of transcript per million mapped reads (FPKM). FPKM normalization divides the read count for each gene by the length of the transcript for that gene, and then, scales all read counts per million reads in the data file. This normalization step allows comparison of expression levels between two genes in the same sample, or of the same gene between different samples. To avoid possible noise of genes expressed at very low levels, only genes expressed above 1 FPKM in at least one sample were considered as "expressed" genes and retained for downstream analysis. Differentially expressed genes (DEGs) were identified using DESeq2, by using as selection parameter adjusted *P*-value lower than 0.01 and Wald test or likelihood ratio test (LRT) for comparison, respectively, of two or more datasets. For K-means clustering analysis, the top 20% most variable genes in at least one of the condition across stimulated and unstimulated neutrophils and monocytes were considered. Gene expression FPKMs were log2-transformed, and for each gene the z score was calculated. Prior to clustering, the optimal number of clusters was estimated using the "clusGap" function of the R package cluster (Tibshirani et al., 2001). Batch effects were removed using the limma package's "removeBatchEffect" function before performing principal component analysis (PCA). PCA was performed on DEGs by using Bioconductor/R package pcaExplorer v.2.10.0. Tracks for the snapshots of the Integrative Genome Viewer (IGV) were generated by using HOMER analysis package. Tracks were linearly rescaled to the same sequencing depth (10 million of mapped reads).

ChIP-seq bioinformatic analysis

Raw sequencing output BCL data were converted to FASTQ files by using the Illumina pipeline software bcl2fastq v2.20. The quality of the reads was checked by FastQC v.0.11.8 (https://www.bioinformatics.babraham.ac.uk/projects/fastqc/). Adaptors and low-quality reads were trimmed by Trim Galore v0.63 using default parameters. To avoid effects derived from different reads lengths, reads were truncated to 51bp using fastx_trimmer from the FASTX-toolkit (http://hannonlab.cshl.edu/fastx_toolkit/). Trimmed reads were mapped to the human genome (Genome Reference Consortium GRCh38, Dec/2013) using Bowtie2 v2.3.5.1 with default parameters (Langmead et al., 2009), and deduplication was performed with markdup of Sambamba v0.6.7. Only reads mapping to the nuclear genome were kept for downstream analyses. The FASTQ file of OCT2-ChIP-seq performed in the GM12878 lymphoblastoid

cell line (for the ENCODE Project Consortium, 2011) was downloaded from the UCSC database (http://genome.ucsc.edu/cgi-bin/hgFileSearch) (2011) and aligned exactly as described for our samples. Tracks were generated and were linearly rescaled to the same sequencing depth (10 million of mapped reads), by using HOMER analysis package.

Identification of TF peaks in ChIP-seqs

PU.1, C/EBPβ and OCT2 peaks were identified using MACS2 v2.2.6 with the following parameters –gsize hs -p 1e-4 –fix-bimodal –call-summits, peaks that overlap with ENCODE blacklist regions were removed with bedtools v2.26.0. ChIP-seq biological replicates peaks were then combined using MSPC (Jalili et al., 2015), with the following parameters -r biological -s 1E-10 -w 1E-6 -m Highest -c 2. ENCODE OCT2 ChIP-seq peaks calling as described above and experiment-matched input DNA was used as control. When overlapping peaks were present among replicates, we assigned to the consensus peak the p value of the most significant peak, as defined by MACS2.

Identification of H3K27Ac-enriched regions by ChIP-seq

H3K27Ac-enriched regions were identified by MACS2 with parameters –gsize hs–broad –broad-cutoff 0.1 –nomodel –extsize 146. Peaks overlapping ENCODE blacklist regions were removed and biological replicates were combined by MSPC to construct consensus peaks. Consensus H3K27Ac coordinates were re-centered to the best nucleosome free regions (NFR) within a 200 bp window, using the command "getPeakTags –nfr" from HOMER package, and then resized to 2 kb as performed by Heinz et al. (2013). Transcription factors and histone modification regions were assigned to genes with the "nearest TSS" criteria. Annotated positions for promoters, exons, introns and other genomic features were based on Human transcriptome annotation (GRCh38v96 ENSEMBL)

Differential peak analysis

Differential H3K27ac occupancy and TFs binding (|log2[fold change]| > 1) and false discovery rare < 0.01 was performed using Bioconductor/R DiffBind (Ross-Innes et al., 2012) v2.14 package (https://bioconductor.org/packages/release/bioc/html/DiffBind.html). The list of consensus TFs as well as H3K27Ac peaks in untreated (n = 2) and R848-treated (n = 2) neutrophils and the corresponding ChIP-seq BAM files, were used as the input data for the analysis. Briefly, overlaps of peaks were examined to determine how well similar samples cluster together with the function dba.count. Second overlaps reads in each interval for each unique sample were counted with the function dba.contrast. Third, a contrast is established and the core analysis of DiffBind was executed by default using DESeq with the function dba.analyze. Finally, the results were reported the function dba.report. The number of tags was counted within a window corresponding to the median width of the peaks or 1000 bp region, for TF peaks or H3K27Ac NFRs, respectively. The peaks changing less than 2 fold change under the two conditions were defined as "common" (Heinz et al., 2010). *De novo* motif discovery analysis of NFRs has been performed using HOMER, essentially as described by Heinz et al. (2010).

Scatterplots and heatmaps

Scatterplots were created by counting around the summit of consensus peaks, within a fixed window corresponding to the median width of the peaks for each TF ChIP-seq, mean tags value (log_2) obtained from resting and R848-treated cells were then plotted as x,y coordinates. For H3K27Ac, ChIP-seq tags were counted within 2 kb from the best NFR. ChIP-seq heatmaps were generated with deeptools v.3.4.3 (Ramírez et al., 2016) using the plotHeatmap function.

Gene ontology (GO) enrichment analysis

Gene ontology enrichment analysis for differential H3K27Ac and TF peaks was performed using the Genomic Regions Enrichment of Annotations Tools (GREAT) (McLean et al., 2010). H3K27Ac and TF bound-regions were assigned to nearby protein-coding genes based on GREATs "basal plus extension rule" for regulatory regions and the whole hg38 genome as background (McLean et al., 2010).

Gene ontology (GO) of differentially expressed genes

All annotated genes resulting from the RNA-seq analysis of resting and R848-stimulated neutrophils were considered as "background gene list," while the upregulated genes were investigated as "input gene list." GO enrichment analysis was performed by the Bioconductor/R package clusterProfiler (version 3.14.3) (Yu et al., 2012) with predefined parameter sets on the available ontologies, i.e., biological processes, molecular functions, and cellular compartments.

Integrative analysis of OCT2 ChIP-seq and expression data

Combined analysis of OCT2 ChIP-seq and transcriptomic data was performed using BETA software (Wang et al., 2013). The BETA-basic subprotocols with –da 1 –df 0.01 –c 0.001 parameters were used to predict the active or repressive function of OCT2, and to identify the candidate target genes that are transcriptionally regulated by OCT2 in response to TLR8 activation (Wang et al., 2013).

Gene set enrichment analysis (GSEA)

GSEA is used to test if a defined set of genes (GeneSet) shows concordant and significant differences between two biological states of cells, whose transcripts are ranked based on their differential expression (Expression dataset) (Subramanian et al., 2005). In this

work, the top 500 genes with the highest BETA score in R848-stimulated human neutrophils were used as GeneSet, while the difference in gene expression levels between si-OCT2 and si-CTRL neutrophil-differentiated HL-60 cells treated with R848 were considered as expression dataset. GSEA 3.0 tool provided by the Broad Institute (https://www.gsea-msigdb.org/gsea/) was used to perform these analyses. All basic and advanced fields were set to default except the ''Permutation type,'' which was set to ''gene_set.'' GSEA enrichment results were reported as normalized enrichment score (NES), whereas false discovery rate (FDR) values smaller than 0.05 were considered significant.

Statistical analysis

Statistical evaluation was performed using one-way or two-way analysis of variance, followed by Tukey's or Bonferroni's post hoc test, respectively. Values of $p < 0.05$ were considered statistically significant. Data are expressed as means ± SE or means ± SD.